

Robust Route Planning for Sidewalk Delivery Robots

Xing Tong^a and Michele D. Simoni^{*a}

^aDivision of Transport and Systems Analysis, KTH Royal Institute of Technology,
Teknikringen 10A, Stockholm 10044, Sweden

July 17, 2025

Abstract

Sidewalk delivery robots are a promising solution for urban freight distribution, reducing congestion compared to trucks and providing a safer, higher-capacity alternative to drones. However, unreliable travel times on sidewalks due to pedestrian density, obstacles, and varying infrastructure conditions can significantly affect their efficiency. This study addresses the robust route planning problem for sidewalk robots, explicitly accounting for travel time uncertainty due to varying sidewalk conditions. Optimization is integrated with simulation to reproduce the effect of obstacles and pedestrian flows and generate realistic travel times. The study investigates three different approaches to derive uncertainty sets, including budgeted, ellipsoidal, and support vector clustering (SVC)-based methods, along with a distributionally robust method to solve the shortest path (SP) problem. A realistic case study reproducing pedestrian patterns in Stockholm’s city center is used to evaluate the efficiency of robust routing across various robot designs and environmental conditions. The results show that, when compared to a conventional SP, robust routing significantly enhances operational reliability under variable sidewalk conditions. The Ellipsoidal and DRSP approaches outperform the other methods, yielding the most efficient paths in terms of average and worst-case delay. Sensitivity analyses reveal that robust approaches consistently outperform the conventional SP, particularly for sidewalk delivery robots that are wider, slower, and have more conservative navigation behaviors. These benefits are even more pronounced in adverse weather conditions and high pedestrian congestion scenarios.

1 Introduction

The last-mile delivery problem represents one of the most challenging aspects of modern logistics due to its cost, increased traffic congestion, and environmental impacts, particularly in urban areas (Boysen et al., 2021). The growing demand for e-commerce and the need for faster and more reliable deliveries have led to the development of innovative solutions such as drones and autonomous ground robots (Jennings and Figliozzi, 2019).

Sidewalk robots, despite their lower speeds and reliance on the existing infrastructure network, represent a safer and higher-capacity solution than drones, making them more appropriate for urban environments. For this reason, several pilot tests have been run for mail and food delivery services by different logistics operators (Bishop, 2016; Burns, 2016). Robots can be deployed as stand-alone units, departing from restaurants, dark kitchens, or depots, or they can operate in combination with trucks to optimize the last mile of delivery. In the latter case, robots can be deployed from the back of the vans to reach the customer (Hossain, 2022). Several companies are considering deploying autonomous delivery robots and have started partnerships with high-tech companies and manufacturers to provide delivery services at the curbside in commercial areas (Wahlberg, 2024), university campuses (Coldewey, 2019), and airports (Bliss, 2023). In recent years, this new delivery option has gained significant interest also within the academic field.

While sidewalk delivery robots operate at relatively low speeds, their efficiency can be significantly affected by factors like pedestrian traffic, terrain, road conditions, obstacles, and weather (Heimfarth

*Corresponding author. Email: micheles@kth.se

et al., 2022). These external variables introduce substantial travel time uncertainty, a challenge that has not been thoroughly addressed in previous studies on robot-based delivery. Existing approaches relying on static travel times for sidewalks may lead to suboptimal operational and strategic decisions (e.g., routing, assignment, location problems) by overlooking potential delays.

In this study, we address robust path planning for sidewalk delivery robots by explicitly considering uncertainty. Unlike “traditional” shortest path problems, we integrate robust and distributionally robust methods with pedestrian simulation to capture realistic sidewalk interactions. Specifically, pedestrian simulation is adopted to generate realistic sidewalk travel times resulting from the interaction between the robot and pedestrian flows, and obstacles at a detailed level. These datasets inform the definition of multiple uncertainty representations required to solve the Robust Shortest Path Problem (RSPP) and Distributionally Robust Shortest Path Problem (DRSP). Two widely-adopted approaches, interval-budgeted and ellipsoidal, and an advanced data-driven method, the kernel-based support vector classification (SVC), are investigated to define uncertainty sets in the RSPP. A realistic urban pedestrian simulation scenario, set in a central district of Stockholm, Sweden, is used to analyze the performance of alternative methods over conventional approaches. This area was designated as a Class 3 clean air zone, a policy aimed at drastically reducing urban vehicle emissions by permitting only fully electric vehicles, making it particularly relevant for studying sidewalk robot delivery (Stockholm County, 2025). In the second part of the paper, we conduct a comprehensive analysis of how design-related factors (e.g., robot maximum speed, size, navigation behavior) and environmental factors (e.g., pedestrian flows, weather) affect the efficiency of robust versus conventional routing.

The main contributions of this study are threefold. First, we investigate the robust route planning problem for sidewalk robot navigation, which, to the best of our knowledge, is the first study of its kind. To capture the complexity of real-world conditions, this optimization framework is integrated with a realistic simulation, allowing us to reproduce the effects of obstacles and pedestrian flows and to generate realistic travel times. Second, we propose a data-driven approach to derive uncertainty sets in the RSPP, the kernel-based SVC, which minimizes assumptions and parameter tuning to endogenously balance conservatism and efficiency. This approach is benchmarked against the more standard budgeted and ellipsoidal uncertainty sets, and the distributionally robust shortest path, to highlight their relative strengths and weaknesses under the comprehensive evaluation framework we proposed for robust routing methods. Third, we investigate the overall performance of robust routing on sidewalk networks through a systematic sensitivity analysis of critical factors, such as robot speed, size, maneuverability, pedestrian flows, and weather conditions.

The remainder of this paper is structured as follows. Since the research fields of robot operational planning and robust route planning are distinct, we briefly review the relevant literature for each in Section 2. Section 3 introduces the methodological approach, covering the three different robust optimization approaches and sidewalk robot simulation. Section 4 provides a detailed explanation of the Stockholm case study, and analyzes the efficiency of robust optimization approaches under various conditions through sensitivity analyses. Section 5 concludes the study by summarizing key insights and outlining avenues for future research.

2 Related studies

2.1 Sidewalk autonomous delivery robots

Sidewalk Autonomous Delivery Robots (SADRs) represent one of the three categories of Autonomous Delivery Robots (ADRs) employed for delivery applications, together with Road Autonomous Delivery Robots (RADRs) and Autonomous Delivery Vehicles (ADVs), as outlined by Sharan et al. (2022) who provide a comprehensive overview of robot-related studies. SADRs are pedestrian-sized robots designed to travel on sidewalks to deliver items autonomously. In this review, the focus is specifically on SADRs, which are referred to as delivery robots for simplicity.

Jennings and Figliozzi (2019) conducted an in-depth study on robots, discussing current regulations and their technical capabilities, and proposed a model to investigate their impact in truck-robot routing problems. Their findings suggest that adopting robots can significantly reduce delivery times, on-road vehicle travel, and costs in comparison to conventional deliveries, particularly in densely populated urban areas. Similar conclusions were drawn by Lemardelé et al. (2021) who estimated the operations costs and external impacts of delivery robots through case studies in Paris, France, and Barcelona,

Spain. Furthermore, Marks (2019) conducted a detailed analysis of the regulatory framework around delivery robots in the US.

The most common research focus for SADR is the truck-robot routing problem, also named as the Traveling Salesman Problem with Robots (TSP-R), which leverages the bulk transportation capabilities of trucks with the flexibility and efficiency of small robots that handle the last mile of deliveries. While the problem can be considered as a particular case of the Traveling Salesman Problem with Drones (TSP-D), the use cases for robots differ significantly. From an operational perspective, robots have notably slower speeds (5–10 km/h compared to 50–100 km/h) and can travel shorter distances (5–10 km compared to 10–30 km). These differences make robots particularly effective for delivering low-value items in densely populated urban environments (Simoni et al., 2020). Different ways to combine trucks and robots in delivery have been discussed by many researchers. Boysen et al. (2018) explored scheduling models specifically for truck-based robot delivery. Their research highlights the potential benefits of using trucks as launching platforms for robots, which can then autonomously deliver goods to customers and return to centralized depots. Liu et al. (2021) developed a two-tier model in which vehicles transfer parcels from depots to satellites in the first tier and robots deliver parcels from satellites to customers in the second tier. Chen et al. (2021) investigated a vehicle routing problem with time windows and delivery robots (VRPTWDR), which focuses on the benefits of deliveries made by both trucks and robots. Their work considers the case that customers need to be present to pick up the parcels when the robots arrive. However, their models are limited by sequential delivery actions of trucks and robots, which means trucks and robots can not make deliveries in parallel. Building on this, Heimfarth et al. (2022) proposed a mixed truck-robot delivery system, introducing additional flexibility by allowing trucks to deliver larger or sensitive packages, while robots handle smaller parcels. Their mixed truck-robot routing problem demonstrated significant cost reductions compared to traditional truck-only or truck-and-robot systems without simultaneous deliveries by both truck and robots within the same tour. Similarly, Murray and Chu (2015) investigated synchronized truck-UAV deliveries, where the UAV is launched from and retrieved by the truck. This formulation laid the foundation for a growing body of research on hybrid truck-drone routing.

Several studies have developed frameworks for robot-only delivery, where parcels are transported exclusively by a fleet of robots without relying on vehicles like trucks or vans. However, these frameworks often encompass various types of delivery robots, not limited to sidewalk robots. Ulmer and Streng (2019) considered a scenario in which ADRs are dispatched directly from depots to pickup stations, and analyzed the operational level of same-day delivery with pickup stations and ADRs. Li et al. (2021) proposed a collaboration framework between ADRs and couriers, where the ADRs transfer parcels between the couriers and the depot, and thus, the couriers can keep making deliveries without returning to the depot. Extending beyond traditional ADRs, Ensafian et al. (2023) investigated a two-echelon network involving autonomous mobile lockers (AMLs) working in coordination with couriers. Their model allows open routes and multi-trip missions, improving operational flexibility and reducing delivery costs. Beyond human-robot collaboration, multimodal delivery models have also been explored. De Maio et al. (2024) formulated a routing problem in which ADRs autonomously synchronize with scheduled public transport lines to reach otherwise inaccessible customers, demonstrating significant cost and emission savings.

The operation of sidewalk robots may lead to potential conflicts with pedestrians, as they must share the same sidewalk space. Gehrke et al. (2023) observed that SADR prompted pedestrians to alter their paths to avoid collisions, with the help of field-recorded video data from a university campus. Additionally, SADR spend 30% of their transit time waiting for pedestrians according to the study of Jennings and Figliozzi (2019). These interactions between robots and pedestrians were taken into account in the sidewalk robot navigation approach proposed by Du et al. (2019).

Despite these advances, existing research assumes static or simplified travel conditions for the sidewalk robot routing problems, overlooking the impact of variable sidewalk travel times due to congestion and other factors. Robots, which typically travel at pedestrian speeds, may face significant delays when navigating crowded or obstructed sidewalks. The traditional shortest path considering length or fixed travel time may not perform effectively in all scenarios, especially when extreme conditions occur. This issue remains insufficiently addressed in the current sidewalk network robot routing problems. This paper addresses this gap by incorporating variable travel times for sidewalk robot delivery in congested areas, providing a more realistic and robust approach for robot-based last-mile delivery operations.

2.2 Robust and distributionally robust shortest path problem

The shortest path problem (SPP) is a fundamental problem in combinatorial optimization and graph theory that aims to find the most efficient route between two (or more) nodes in a network. It has broad applications in various fields, including transportation, planning, and network design (Kumawat et al., 2021). However, real-world network conditions are often uncertain due to fluctuating travel times, changing road conditions, or unpredictable delays. To address these uncertainties, the robust shortest path problem (RSPP) extends the classical SPP by incorporating uncertainty into the model, ensuring that the chosen path remains effective even under adverse conditions.

Robust Optimization (RO) approaches typically handle uncertainty by defining uncertainty sets that capture possible variations in arc costs or travel times. Commonly used types of uncertainty sets include convex hull (Kasperski and Zielinski, 2016), intervals (Chassein and Goerigk, 2015), ellipsoid (Ben-Tal and Nemirovski, 1998), budgeted uncertainty (Goerigk and Schöbel, 2015) and permutohull (Bertsimas and Brown, 2009). Each of these sets reflects different assumptions about the nature of uncertainty and requires distinct optimization techniques to solve the RSPP efficiently. These different types of uncertainty sets were tested by Dokka and Goerigk (2017) using real-world traffic measurements, and compared their performance under different performance indicators. Chassein et al. (2019) built and compared a range of uncertainty sets, and developed an efficient solution algorithm focusing on the case of ellipsoidal uncertainty for RSPP. Different studies extended to solve more complex problems, such as the RSPP with time windows (Alves Pessoa et al., 2015), and to explicitly account for accident probability and the accident consequence (Kwon et al., 2013).

In recent years, data-driven approaches have moved beyond traditional uncertainty modeling by incorporating empirical insights, allowing for the dynamic adjustment to better align with observed variability and real-world trends. A growing body of research has investigated the distributionally robust shortest path problem (DRSP), where an ambiguity set (i.e., a collection of plausible cost distributions) is constructed based on the empirical distribution derived from data (Cheng et al., 2013; Wang et al., 2019; Ketkov et al., 2021). Although DRSP provides theoretical robustness guarantees, it is often constrained by the limited expressiveness of its uncertainty sets and can be computationally challenging for large-scale networks or high-dimensional settings. An alternative is to adopt machine learning techniques, which can better capture the complexity and asymmetry of real-world data. For example, Shang et al. (2017) proposed a Support Vector Clustering (SVC) to construct uncertainty sets, and later extended this method to handle high-dimensional uncertainty with decomposition techniques ((Shang and You, 2018)). These approaches can effectively handle data correlation and asymmetry, but since they are Single-Kernel Learning-based (SKL) methods in essence, their performance heavily depends on projection directions, and they may lead to over-conservative solutions, particularly for asymmetric data. Han et al. (2021) proposed a Multiple-Kernel Learning-based (MKL) SVM approach that optimally selects projection directions to create non-conservative polyhedral uncertainty sets. However, this method is only suitable for low-dimensional uncertainty. Ghiasvand and Rahmani (2023) developed a weighted one-class support vector machine (WOC-SVM) algorithm, in order to create adjustable uncertainty sets considering supplementary information, such as predicted values. Goerigk and Kurtz (2023) adopted deep neural networks to construct non-convex uncertainty sets, and integrated them into a robust optimization model by formulating the adversarial problem as a convex quadratic mixed-integer program. These advances demonstrate the potential of machine learning techniques, but still face computational challenges, especially for high-dimensional and large datasets. Roytvand Ghiasvand et al. (2024) addresses this problem by decreasing the number of support vectors through a novel hybrid two-stage clustering (TSC) algorithm.

In this paper, we develop two data-driven methods to specifically address the robust routing planning in sidewalk robot delivery: a Wasserstein-based DRSP approach and a RSP method using SKL-based and MKL-based SVC approaches combined with the TSC algorithm. We evaluate and compare the performance of these methods against two established baselines through realistic simulation scenarios designed for sidewalk robot delivery.

3 Methodological approach

In this study, we systematically evaluated the performance of four approaches: Budgeted uncertainty, Ellipsoidal uncertainty, Kernel-based SVC uncertainty, and Wasserstein ambiguity. These methods are

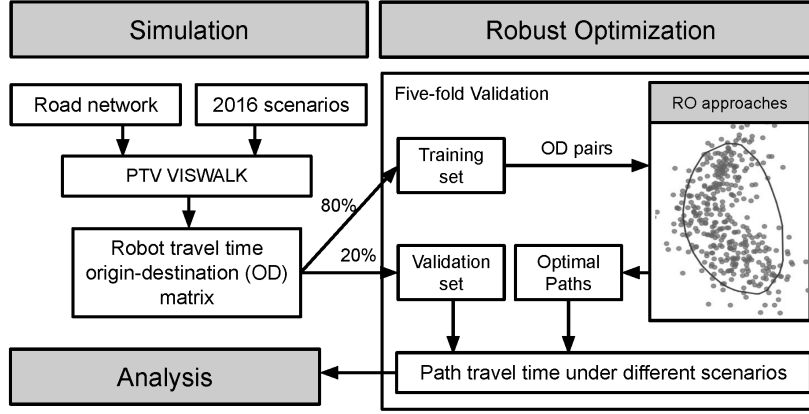


Figure 1: Framework for Simulation and Optimization

assessed in the context of sidewalk robot delivery using pedestrian simulation data.

Budgeted uncertainty, introduced by (Bertsimas and Sim, 2003), is a widely recognized and commonly adopted approach for RSPP, appearing extensively in both theoretical research and practical applications. It is computationally tractable and provides a tunable trade-off between robustness and conservatism. Ellipsoidal uncertainty typically provides stable solutions and performs well overall. It achieves the best trade-off compared to other approaches, including convex hull, intervals, budgeted, permutohull, and symmetric permutohull uncertainty, when applied to RSPP with real-world data Chassein et al. (2019).

The first two approaches serve as traditional baselines. In contrast, the latter two are more recent data-driven methods. Kernel-based SVC uncertainty leverages machine learning to construct uncertainty sets from data but remains underexplored in the context of RSPP, especially for sidewalk robot delivery. We implement and evaluate two variants of this method: SKL-based SVC and MKL-based SVC. Additionally, we include the Wasserstein-based DRSP method, a prominent data-driven technique that offers strong theoretical guarantees and flexible ambiguity set construction based on empirical distributions.

The framework of the integration of simulation and optimization is shown in Figure 1. An overview of the four approaches is provided in Section 3.1. This is followed by the introduction of the model used to simulate the sidewalk robots in Section 3.2.

3.1 Robust route planning approaches

In the classic shortest path problem, we denote a directed graph as $G = (V, A)$ where V indicates the set of vertices or nodes, and A indicates the set of segments, $|A| = n$. Each segment has a cost c . Given a start point s and a target point t , the goal is to find a route with a minimum sum of costs between them. This problem can be defined briefly as follows:

$$\min\{\mathbf{c}^T \mathbf{x} : \mathbf{x} \in X\} \quad (1)$$

where X is the set of feasible paths defined by standard flow conservation and binary constraints from s to t , and $X \subseteq \{0, 1\}^n$.

In the robust shortest path problem, the segment costs c are not precisely known. There is a set of observations of costs $D = \{\mathbf{c}^1, \dots, \mathbf{c}^N\}$, where N is the number of observations and $\mathbf{c}^i \in \mathbb{R}^n$. We use the notation $[n] = \{1, 2, \dots, n\}$ and $[N] = \{1, 2, \dots, N\}$. Based on the set of observations D , the uncertainty set U can be modeled. The RSPP is then denoted as:

$$\min\{\max_{\mathbf{u} \in U} \mathbf{u}^T \mathbf{x} : \mathbf{x} \in X\} \quad (2)$$

which means finding the shortest path in X considering the worst case in U .

In this section, four robust route planning approaches are employed for sidewalk robot delivery, generating three different types of uncertainty sets and one ambiguity set. A visual example for each approach using a randomly generated dataset is shown in Figure 2. This dataset contains 400 two-dimensional samples generated from a mixture of Gaussian distributions.

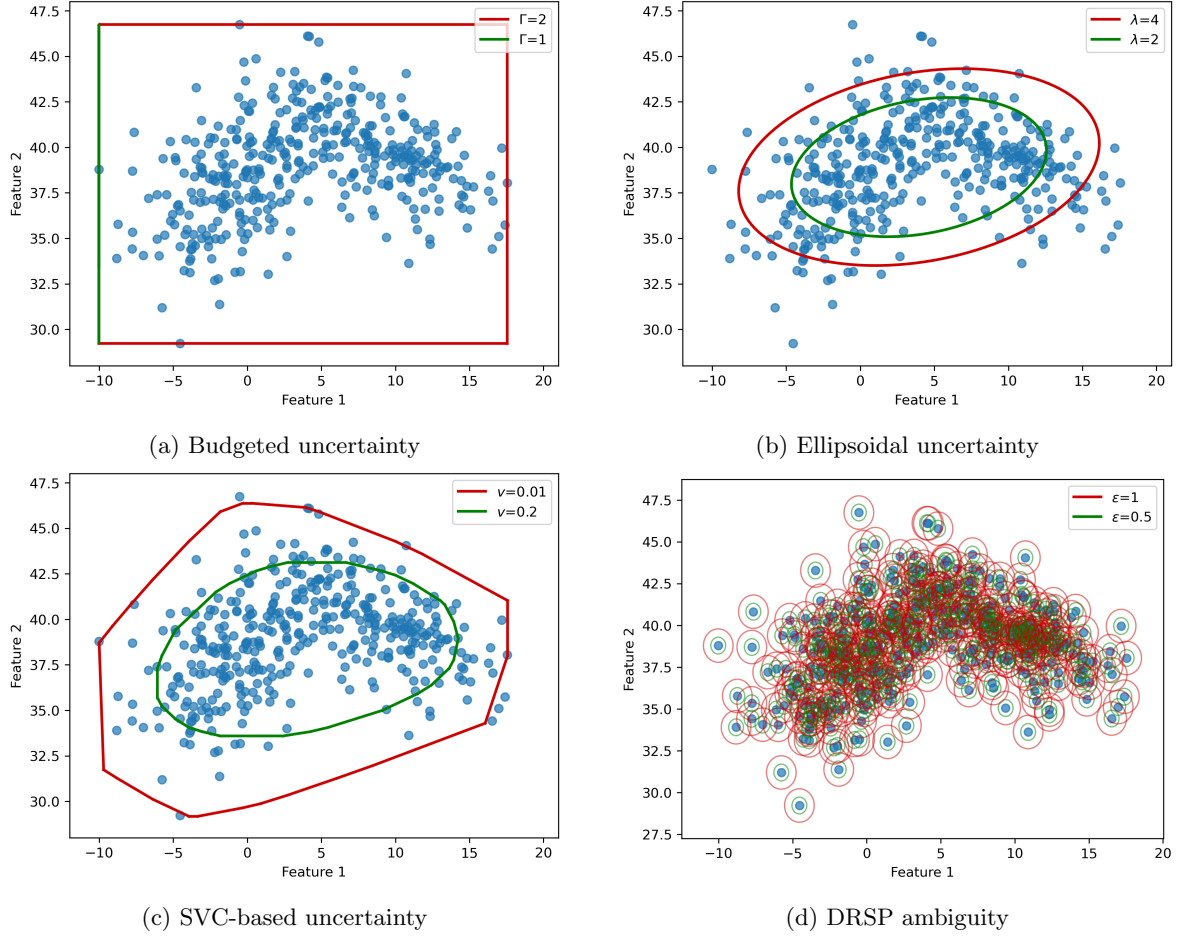


Figure 2: Visual examples for four robust methods

3.1.1 Budgeted uncertainty

The Budgeted uncertainty approach (Bertsimas and Sim (2003)) for robust discrete optimization involves defining each entry $u_j, j \in [n]$ within the interval $[\underline{c}_j, \underline{c}_j + d_j]$. In the case of RSPP, u_j represents the robust cost at certain segment j , \underline{c}_j is the minimum observed cost of segment j , and d_j denotes the deviation between maximum cost and minimum cost. The degree of conservatism is controlled by the parameter Γ (Figure 2a) which restricts at most $\Gamma \in \{1, 2, \dots, n\}$ to take values in the interval, while the remaining entries take the minimum values. If $\Gamma = 0$, the influence of the cost deviations is completely ignored. The budgeted uncertainty set is expressed as:

$$U^B = \left\{ \mathbf{u} \left| \begin{array}{l} \underline{c}_j \leq u_j \leq \underline{c}_j + d_j \lambda_j, \forall j \in [n] \\ \sum_{j \in [n]} \lambda_j \leq \Gamma, \lambda_j \in \{0, 1\} \end{array} \right. \right\} \quad (3)$$

This problem can be formulated as:

$$\begin{aligned} \min \quad & \underline{\mathbf{c}}\mathbf{x} + \max_{\{S|S \subseteq [n], |S| \leq \Gamma\}} \sum_{(p,q) \in S} d_{pq} x_{pq} \\ \text{s.t.} \quad & \mathbf{x} \in X \end{aligned} \quad (4)$$

The constraints here refer to the shortest path problem. Finding such a robust solution is NP-hard, but this problem can be solved by solving at most $n+1$ nominal shortest path problems (Bertsimas and Sim, 2003). This algorithm allows modelers to balance cost and robustness by adjusting the parameter Γ .

3.1.2 Ellipsoidal uncertainty

The Ellipsoidal uncertainty (Ben-Tal and Nemirovski, 1998, 1999) encompasses various reasonable types of ellipsoids and the intersections of finitely many ellipsoids. They make the corresponding robust convex program a tractable problem. An ellipsoidal uncertainty set can be in the form of

$$U^E = \{\mathbf{u} : (\mathbf{u} - \hat{\mathbf{c}})^T \boldsymbol{\Sigma}^{-1} (\mathbf{u} - \hat{\mathbf{c}}) \leq \lambda\} \quad (5)$$

where $\lambda \geq 0$ is a parameter controlling the size of the ellipsoid (Figure 2b). Here $\hat{\mathbf{c}}$ and $\boldsymbol{\Sigma}$ are generated from observed points considering the best fit of multivariate normal distribution $N(\hat{\mathbf{c}}, \boldsymbol{\Sigma})$:

$$\hat{\mathbf{c}} = \frac{1}{N} \sum_{i \in [N]} \mathbf{c}^i \quad (6)$$

$$\boldsymbol{\Sigma} = \frac{1}{N} \sum_{i \in [N]} (\mathbf{c}^i - \hat{\mathbf{c}})(\mathbf{c}^i - \hat{\mathbf{c}})^T \quad (7)$$

In ellipsoidal uncertainty, they represent the center of the ellipsoid as well as the shape and the size of the ellipsoid respectively. The resulting robust shortest path problem under ellipsoidal uncertainty can be denoted as (Dokka and Goerigk, 2017):

$$\begin{aligned} \min \quad & \hat{\mathbf{c}}^T \mathbf{x} + z \\ \text{s.t.} \quad & z^2 \geq \lambda (\mathbf{x}^T \boldsymbol{\Sigma} \mathbf{x}) \\ & \mathbf{x} \in X \end{aligned} \quad (8)$$

The term z here is an auxiliary variable to account for the worst-case impact of the uncertainty set.

3.1.3 Kernel-based SVC uncertainty

The SKL-based SVC uncertainty approach (Shang et al., 2017) is a data-driven approach that combines an unsupervised machine learning algorithm, the SVC, with the Weighted Generalized Intersection Kernel (WGIK) method. It utilizes Support Vectors (SV) to define boundaries in feature space, grouping data points into clusters by finding the smallest sphere that encloses them. The kernel function WGIK is calculated in Eq. (9):

$$K(\mathbf{u}, \mathbf{v}) = \sum_{k=1}^n l_k - \|\mathbf{Q}(\mathbf{u} - \mathbf{v})\|_1 \quad (9)$$

where \mathbf{Q} is a weighting matrix generated from covariance matrix $\mathbf{Q} = \boldsymbol{\Sigma}^{-\frac{1}{2}}$. This kernel function is concave, ensuring a convex acceptance region for the SVC.

This SKL-based SVC approach not only manages correlated uncertainties, resulting in asymmetric uncertainty sets, but it also features adaptive complexity, embodying a nonparametric approach. The resulting convex polyhedral uncertainty set can ensure the robust counterpart problem of the same type as the deterministic problem. The explicit expression of this uncertainty set can be derived as a set of linear inequalities:

$$U^{SVC} = \left\{ \mathbf{u} \left| \begin{array}{l} \exists \mathbf{v}_i, i \in SV \text{ s.t.} \\ \sum_{i \in SV} \alpha_i \cdot \mathbf{1}^T \mathbf{v}_i \leq \theta \\ -\mathbf{v}_i \leq \mathbf{Q}(\mathbf{u} - \mathbf{u}^i) \leq \mathbf{v}_i, \forall i \in SV \end{array} \right. \right\} \quad (10)$$

where α are Lagrangian multipliers, and \mathbf{v}_i are auxiliary variables introduced. SV refers to a list of support vectors, the number of which is controlled by a predefined regularization parameter $v \in (0, 1]$. It is an upper bound on the fraction of outliers and a lower bound on the fraction of support vectors (Figure 2c). It is introduced to control the conservatism degree of the uncertainty set.

Before applying the above SKL-based SVC uncertainty set into the robust shortest path problem, Eq.(2) can be first simplified by moving the inner objective function into a constraint:

$$\begin{aligned} \min_{\mathbf{x} \in X, b} \quad & b \\ \text{s.t.} \quad & \max_{\mathbf{u} \in U} \mathbf{u}^T \mathbf{x} \leq b \end{aligned} \quad (11)$$

Then the linear inequality constraints in Eq.(10) can replace the uncertainty set U in the left-hand side (LHS) of the constraint in Eq. (11). After introducing Lagrange multipliers, the final model for the robust shortest path problem with WGIK-SVC-based uncertainty set can be defined as follows:

$$\begin{aligned}
& \min_{x_{pq}, \lambda_i, \mu_i, \eta, \beta} && b \\
& \text{s.t.} && \sum_{i \in SV} (\mu_i - \lambda_i)^T \mathbf{Q} \mathbf{u}^i + \eta \theta \leq b \\
& && \sum_{i \in SV} \mathbf{Q} (\lambda_i - \mu_i) + \mathbf{x} = \mathbf{0} \\
& && \lambda_i + \mu_i = \eta \cdot \alpha_i \cdot \mathbf{1}, \forall i \in SV \\
& && \lambda_i, \mu_i \in \mathbb{R}_+^n, \eta \geq 0, \mathbf{x} \in X
\end{aligned} \tag{12}$$

The detailed introduction of SKL-based SVC and derivation of Eq.(12) is provided in Appendix A.

This WGIK-based SVC approach still achieves high computational efficiency by formulating the robust counterpart problem as the deterministic problem even if it generates $2 * |SV| * |A| + 1$ additional variables. However, its computational tractability is lost when applied to the RSPP. The RSPP with kernel-based SVC uncertainty is Mixed-Integer Programming (MIP) with both continuous variables (Lagrange multipliers) and binary variables (path choices), and usually has many data points (large $|SV|$) and high dimensions (large $|A|$). This makes this problem computationally intensive and hard to find a solution efficiently even under a small road network. In addition, the SVC is impacted by the curse of dimensionality, suggesting that the accuracy of the resultant data-driven uncertainty sets may decline when dealing with high-dimensional uncertainties (Ning and You, 2018). This is particularly evident in RSPP because of high dimensions.

To tackle the aforementioned challenges, the Two-Stage Clustering with Dimensional Separation (TSC-DS) algorithm proposed by Roytvand Ghiasvand et al. (2024) is employed. Unlike other methods to overcome the curse of dimensionality, such as Principal Component Analysis (PCA) which is used for highly correlated datasets as described in (Shang and You, 2018), the TSC-DS algorithm is specifically developed for column-wise uncertainty. This algorithm not only significantly reduces the number of SVs, but also decreases the number of dimensions. At the first stage, it eliminates additional SVs that do not contribute to the uncertainty set construction using the SKL-based SVC approach. The remaining dataset is then divided into F low-dimensional subsets. At the second stage, the SVC uncertainty set $U_f^{SVC}, f \in [F]$ for each subset is constructed. Each uncertainty set U_f^{SVC} can be written as:

$$U_f^{SVC} = \left\{ \mathbf{u}_f \left| \begin{array}{l} \exists \mathbf{v}_{i_f}, i_f \in SV_f \text{ s.t.} \\ \sum_{i_f \in SV_f} \alpha_{i_f} \cdot \mathbf{1}^T \mathbf{v}_{i_f} \leq \theta_f \\ -\mathbf{v}_{i_f} \leq \mathbf{Q}_f (\mathbf{u}_f - \mathbf{u}^{i_f}) \leq \mathbf{v}_{i_f}, \forall i_f \in SV_f \end{array} \right. \right\} \tag{13}$$

Then the final model Eq.(14) can be reformulated as:

$$\begin{aligned}
& \min_{x_{pq}, \lambda_{i_f}, \mu_{i_f}, \eta_f} && b \\
& \text{s.t.} && \sum_{f \in [F]} \left(\sum_{i_f \in SV_f} (\mu_{i_f} - \lambda_{i_f})^T \mathbf{Q}_f \mathbf{u}^{i_f} + \eta_f \theta_f \right) \leq b \\
& && \sum_{i_f \in SV_f} \mathbf{Q}_f (\lambda_{i_f} - \mu_{i_f}) + \mathbf{x}_f = \mathbf{0}, \forall f \in [F] \\
& && \lambda_{i_f} + \mu_{i_f} = \eta_f \cdot \alpha_{i_f} \cdot \mathbf{1}, \forall i_f \in SV_f, \forall f \in [F] \\
& && \lambda_{i_f}, \mu_{i_f} \in \mathbb{R}_+^n, \eta_f \geq 0, \mathbf{x} \in X
\end{aligned} \tag{14}$$

It is worth mentioning that the dimensional separation technique employed in the TSC-DS algorithm significantly enhances the applicability of the MKL-based SVC approach. This approach is particularly suitable for managing uncertainty in lower-dimensional spaces, specifically when the number of dimensions is fewer than eight (Han et al., 2021). The advantage of the MKL method lies in its ability to flexibly select and combine multiple kernel functions, optimizing the kernel weights

π_m automatically to best fit the data distribution. In contrast, the SKL method relies on a single pre-specified kernel, which may not sufficiently capture complex structures in high-dimensional or non-linearly separable data.

Han et al. (2021) proposed a concave kernel structure for MKL as an extension of the WGIK function, enabling a more refined construction of uncertainty sets in a robust optimization (RO) framework. The proposed concave kernel function is defined as follows:

$$K_m(\mathbf{u}, \mathbf{v}) = 1 - \left| \frac{\mathbf{q}_m^\top (\mathbf{u} - \mathbf{v})}{c_m \cdot \kappa} \right| \quad (15)$$

where \mathbf{q}_m represents the projection direction, c_m is a normalization factor, κ controls the scaling of the kernel function, and $m \in [M]$, with M representing the number of kernels.

A critical factor in MKL is the regularization parameter μ , which directly controls how many kernels are actively used in constructing the uncertainty set. A lower μ value encourages sparsity, forcing the optimization process to select only a few relevant kernels while setting others to zero. A higher μ value distributes the weight across multiple kernels, increasing complexity.

Building on this foundation, the RO-compatible MKL-based SVC uncertainty set in the second stage of the TSC-DS algorithm can be yielded as:

$$U_f^{MKL-SVC} = \left\{ \mathbf{u}_f \left| \sum_{i_f \in SV_f} \alpha_{i_f}^* \sum_{m_f \in SK_f} \pi_{m_f}^* K_{m_f}(\mathbf{u}_f, \mathbf{u}_{i_f}) \geq \rho_f^* \right. \right\} \quad (16)$$

where SK_f is the set of selected supported kernels for subset f , $\alpha_{i_f}^*$ are the optimized dual variables associated with the SVs, $\pi_{m_f}^*$ are the optimized kernel weight coefficients, which determine the relative importance of different basis kernels, and ρ_f^* is a threshold parameter defining the boundary of the uncertainty set.

Consequently, the RO model for RSP using MKL-based SVC uncertainty can finally be reformulated as:

$$\begin{aligned} \min_{x_{pq}, \lambda_{i_f}, \mu_{i_f}, \eta_f} \quad & b \\ \text{s.t.} \quad & \sum_{f \in [F]} \left(\sum_{i_f \in SV_f} \sum_{m_f \in SK_f} (\mu_{i_f m_f} - \lambda_{i_f m_f}) \frac{\mathbf{q}_{m_f}^\top (o_{i_f})}{c_{m_f} \cdot \kappa_f} + \eta_f (1 - \rho_f^*) \right) \leq b \\ & \sum_{i_f \in SV_f} \sum_{m_f \in SK_f} (\lambda_{i_f m_f} - \mu_{i_f m_f}) \frac{\mathbf{q}_{m_f}}{c_{m_f} \cdot \kappa_f} + \mathbf{x}_f = \mathbf{0}, \forall f \in [F] \\ & \lambda_{i_f m_f} + \mu_{i_f m_f} = \eta_f \cdot \alpha_{i_f}^* \cdot \pi_{m_f}^*, \forall i_f \in SV_f, m_f \in SK_f, \forall f \in [F] \\ & \lambda_{i_f m_f}, \mu_{i_f m_f} \geq 0, \forall i_f \in SV_f, m_f \in SK_f, \forall f \in [F] \\ & \eta_f \geq 0, \forall f \in [F], \mathbf{x} \in X \end{aligned} \quad (17)$$

3.1.4 Distributionally RSP

The other data-driven approach adopted is the DRSP method using Wasserstein ambiguity sets proposed by Wang et al. (2019, 2020). Unlike the aforementioned models, this method does not rely on uncertainty sets capturing all possible variations. Instead, it defines an ambiguity set (i.e., a Wasserstein ball) containing all probability distributions within a specified Wasserstein distance ϵ_N from the empirical distribution. This ambiguity set is derived from finite samples and helps address the uncertainty in travel times. This formulation offers a flexible way to incorporate data-driven uncertainty and control conservatism through the radius ϵ_N , which reflects the confidence in the empirical data (Figure 2d). The optimal path is determined by minimizing the worst-case α -reliable mean-excess travel time (METT), which represents the expected travel time exceeding the α -quantile and accounts for the risk of extreme delays, evaluated over all distributions in the Wasserstein ambiguity set. The formulation of the α -METT for a given path \mathbf{x} under the distribution F is given below:

$$\text{METT}_\alpha(\mathbf{x}) = \min_{t \in \mathbb{R}} \left\{ t + \frac{1}{\alpha} \mathbb{E}_F [\max\{\boldsymbol{\xi}^T \mathbf{x} - t, 0\}] \right\} \quad (18)$$

where $\xi \in \mathbb{R}^n$ is the vector of segment travel times under distribution F , t is the quantile threshold, and $\max\{\xi^T \mathbf{x} - t, 0\}$ measures the excess travel time above threshold t .

Furthermore, this method incorporates support intervals to ensure that perturbed distributions remain realistic. Let $[\mathbf{a}, \mathbf{b}]$ denote the empirical support interval for segments, constructed from the free flow and maximum observed travel times. The Wasserstein DRSP model can be formulated as:

$$\begin{aligned} \min_{t, \mathbf{s}, \boldsymbol{\lambda}, \boldsymbol{\gamma}_i, \boldsymbol{\eta}_i} \quad & t + \frac{1}{\alpha} \left\{ \frac{1}{N} \sum_{i=1}^N s_i + \lambda \epsilon_N \right\} \\ \text{s.t.} \quad & (\mathbf{x} + \boldsymbol{\gamma}_i - \boldsymbol{\eta}_i)^T \hat{\xi}^i - \boldsymbol{\gamma}_i^T \mathbf{a} + \boldsymbol{\eta}_i^T \mathbf{b} - t \leq s_i \\ & \|\boldsymbol{\gamma}_i + \mathbf{x} - \boldsymbol{\eta}_i\|_q \leq \lambda \\ & \boldsymbol{\eta}_i \geq 0, \quad \boldsymbol{\gamma}_i \geq 0, \quad s_i \geq 0, \quad \forall i \in [N] \\ & \mathbf{x} \in X \end{aligned} \tag{19}$$

where $\hat{\xi}^i$ is the i -th sample vector, $\boldsymbol{\eta}_i$ and $\boldsymbol{\gamma}_i$ are Lagrange multipliers for the support set, s_i is a slack variable, and $\|\cdot\|_q$ is the dual norm corresponding to the chosen l_p -norm for the Wasserstein distance. The reformulation of the worst-case METT problem into a tractable mixed 0–1 convex program allows for efficient optimization even under high-dimensional and sample-based uncertainty.

The two key parameters, ϵ_N and α , play crucial roles in controlling the model's robustness and risk sensitivity. The radius ϵ_N governs the size of the Wasserstein ball: increasing ϵ_N leads to a more conservative model by expanding the ambiguity set and allowing for greater deviations from the empirical distribution. Conversely, a smaller ϵ_N tightens the ambiguity set and reduces robustness, relying more heavily on the quality of the data. The parameter α , which appears in the definition of the METT, represents the tail probability level. A smaller α results in a more risk-averse model that penalizes large deviations and extreme outcomes more heavily, potentially increasing the total cost. Larger α values yield a model that is less sensitive to outliers, favoring average-case performance. Therefore, proper tuning of ϵ_N and α is essential for balancing robustness, reliability, and computational efficiency.

3.2 Sidewalk robot simulation

To simulate realistic sidewalk navigation for sidewalk delivery robots, we integrate an agent-based pedestrian simulator, PTV VISWALK (PTV, 2023), that accounts for interactions among pedestrians, robots, and static urban obstacles. VISWALK is based on the Social Force Model (SFM), which reproduces pedestrians movements and interactions at the microscopic level.

The SFM, one of the most prominent models for pedestrian dynamics, was originally proposed by Helbing and Molnar (1995). It describes a pedestrian's motion in the form of an acceleration or deceleration, resulting from a number of different forces acting on the pedestrian such as social, psychological, and physical forces. Given a certain pedestrian, the total force \vec{F} can be expressed as the sum of four terms (PTV, 2023):

$$\vec{F} = \vec{F}_{driving} + \vec{F}_{social} + \vec{F}_{wall} + \vec{F}_{noise} \tag{20}$$

where $\vec{F}_{driving}$ represents the driving force that the pedestrian wants to reach a certain destination as comfortable as possible, \vec{F}_{social} refers to the interaction forces between the pedestrian and other individuals, \vec{F}_{wall} represents the interaction forces between the pedestrian and obstacles, \vec{F}_{noise} is a random force that added to the total social forces if a pedestrian remains below his desired speed for a certain time, to avoid simulated pedestrians getting stuck for periods of time.

$\vec{F}_{driving}$ is described by an acceleration term of the form:

$$\vec{F}_{driving} = \frac{\vec{v}_0 - \vec{v}}{\tau} \tag{21}$$

In this formulation, \vec{v}_0 is the desired speed of the individual, while \vec{v} is the instantaneous speed. The term τ refers to the relaxation time required for the individual to approach the desired speed. A larger τ implies that it takes the pedestrian more time to adjust its velocity.

The original \vec{F}_{social} was extended by Johansson et al. (2008) who introduced an angle-related friction parameter to express the anisotropy in the model. This modification has been implemented

into VISWALK’s SFM by splitting the original \vec{F}_{social} as the sum of isotropic \vec{F}_{soc_iso} and mean social forces \vec{F}_{soc_mean} to consider the the effect of vision field and anisotropy. The isotropic social force that the pedestrian α experiences from another pedestrian β is defined as follows:

$$\vec{F}_{\alpha\beta}^{soc_iso} = A_{soc_iso} w(\lambda) e^{-d_{\alpha\beta}/B_{soc_iso}} \vec{n}_{\alpha\beta} \quad (22)$$

where A_{soc_iso} and B_{soc_iso} are non-measurable parameters controlling the two forces among pedestrians, and d is the distance between the pedestrian α and the influencing pedestrian β . The term \vec{n} refers to the unit vector pointing from the influencing pedestrian β to the influenced pedestrian α . The λ is an anisotropy factor that makes the forces from behind not influence the pedestrian as much as forces in the front. It ranges from 0 to 1 and grows with the strength of interactions from behind. By the function $w(\lambda)$ below, the force is dependent of direction:

$$w(\lambda) = \left(\lambda + (1 - \lambda) \frac{1 + \cos(\varphi)}{2} \right) \quad (23)$$

The φ denotes the angle between the current direction of the pedestrian α and the relative position of the influencing pedestrian β . The overall isotropic social force for pedestrian α is the sum of $\vec{F}_{\alpha\beta}^{soc_iso}$ for all nearby pedestrians β within the range identified by the parameter *react_to_n*, which is used to control the maximum number of persons considered in the closest surrounding.

The formula of mean social forces is similar to that of isotropic social forces:

$$\vec{F}_{\alpha\beta}^{soc_mean} = A_{soc_mean} e^{-d_{\alpha\beta}/B_{soc_mean}} \vec{n}_{\alpha\beta} \quad (24)$$

where A_{soc_mean} and B_{soc_mean} denote the strength and range of the social force respectively. However, all forces that act in the back (180°) of the pedestrians are ignored. Moreover, a parameter VD is introduced to generalize the distance $d_{\alpha\beta}$ in order to take into account the step width of the influencing pedestrian. If $VD = 0$, it will not consider the relative velocities of pedestrians and is equal to the body surface distance between two pedestrians.

\vec{F}_{wall} represents the interaction forces between the pedestrian and obstacles, and is calculated in the same way as \vec{F}_{social} . \vec{F}_{noise} refers to the fluctuation term (Noise) in the original SFM, which is expressed through an acceleration parameter m/s^2 .

While VISWALK’s default parameters represent typical pedestrian behavior, they are adapted here to reflect sidewalk delivery robots, which are expected to move more cautiously in dense environments. Table 1 summarizes the adjusted parameters. Our parameter choices are informed by literature on robot-human interaction in pedestrian environments. Yang et al. (2023) and (Anvari and Wurdemann, 2020) propose extensions of the SFM to predict human trajectories and behavior in the presence of a robot. Meanwhile, research by Ferrer et al. (2013a,b) introduces a social-aware navigation approach by applying the SFM to the robot itself to govern its movement. However, the parameters in their model are not applicable in this study. To date, no study has specifically calibrated SFM parameters for sidewalk robots within VISWALK. Our study builds on previous work by Truong and Ngo (2017), who developed an extended SFM for mobile robot navigation in dynamic and crowded environments.

To align the SFM with sidewalk robot characteristics, four key parameters are adjusted: τ , A_{soc_iso} , B_{soc_iso} , and λ . The relaxation time parameter τ is particularly influential (Gruden et al., 2022; Shi et al., 2021) since it determines how quickly a pedestrian adjusts their current speed and direction to align with their desired speed and direction. Given the conservative design of sidewalk robots, which are expected to react more slowly and cautiously than humans, the default τ value is set to 0.8. The other three parameters align with those used for human repulsive forces in the extended SFM proposed by Truong and Ngo (2017), as shown in Table 1.

Finally, the desired speed of sidewalk robots is fixed at 5 km/h with no deviation, and their size is set to the default size of an adult male in VISWALK, which is 0.538 m wide.

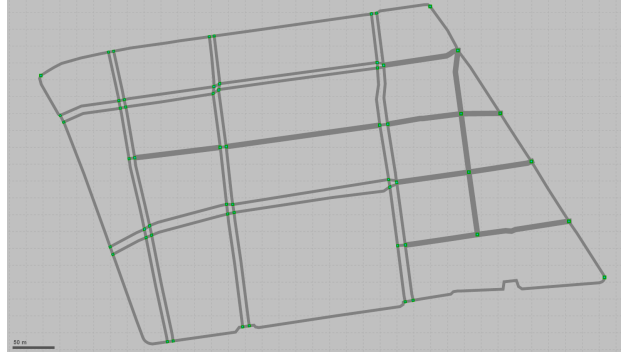
Given the absence of publicly available real-world operational data on sidewalk delivery robots, the simulated robot behavior and interactions depend inherently on design specifications and operational settings defined by robot manufacturers. For this reason, an extensive sensitivity analysis exploring how variations in key robot design affect the performance of robust strategies is provided in Section 4.3.

Table 1: Social force model parameters for pedestrians (default) and robots

Parameter	τ	ReactToN	A_soc _isotropic	B_soc _isotropic	λ	A_soc _mean	B_soc _mean	VD	Noise
Default	0.4	8	2.72	0.2	0.176	0.4	2.8	3	1.2
Robot	0.8	8	2.1	0.35	0.45	0.4	2.8	3	1.2



(a) Network in QGIS



(b) Network in VISWALK

Figure 3: Refined Pedestrian network in Norrmalm, Stockholm

4 Results

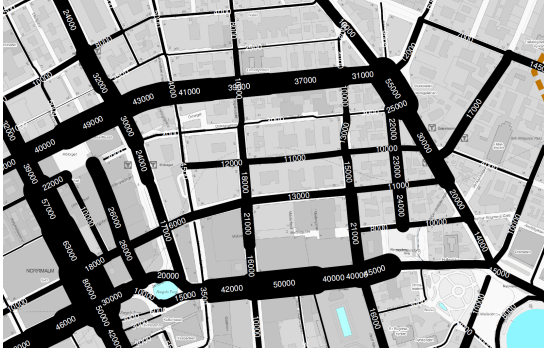
This section focuses on the analysis of robust navigation for sidewalk robot delivery. Section 4.1 describes the setup of a realistic case study based on the urban pedestrian network of central Stockholm. Section 4.2 systematically evaluates the performance of three types of uncertainty sets, Budgeted uncertainty, Ellipsoidal uncertainty, and data-driven SVC uncertainty, offering insights into the trade-off between robustness and efficiency. Section 4.3.1 and Section 4.3.2 provide a comprehensive analysis of how design-related factors and environmental factors affect the efficiency of both traditional routing and robust routing solutions.

4.1 Scenario setup

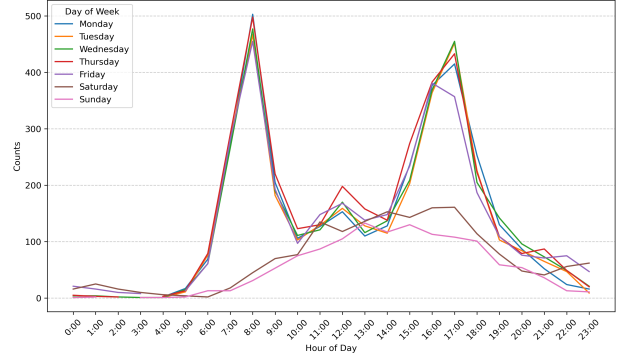
The analysis focuses on a section of Norrmalm, located in central Stockholm, bounded by Kungsgatan, Birger Jarlsgatan, Hamngatan, and Sveavägen. This area was designated as a Class 3 clean air zone which allows only fully electric vehicles. It is also characterized by high pedestrian traffic and complex interactions between obstacles and pedestrians, making it a particularly relevant setting for studying sidewalk robot delivery. The network geometry was obtained from OpenStreetMap and refined using QGIS to ensure accuracy (Figure 3). The network has 99 segments, including 65 sidewalks and 34 crossings. Note that this network size is particularly appropriate for sidewalk delivery robots, since they are designed for last-mile logistics and generally do not undertake long-distance routes. It is both realistic and practical to model a compact, urban network rather than a large-scale city-wide system.

The VISWALK simulation input includes road network geometry, pedestrian demand, behavioral parameters, and obstacles, all calibrated to reflect real-world pedestrian and robot behavior. The simulation duration is set as 900 seconds (15 minutes). Pedestrian origin-destination (OD) matrices are constructed for each hour from 10 a.m. to 10 p.m. (12 hours) across 7 days of the week. These are combined with 12 distinct obstacle configurations and bidirectional travel for each segment, resulting in a total of 2016 simulation scenarios. An additional scenario without obstacles or pedestrians is simulated to obtain the free flow travel time for each segment.

The pedestrian daily traffic volumes data were obtained from openly available data shared by Stockholm municipality (Stockholms County, 2017). This resource provides a detailed flow map showing the average number of pedestrians per day on streets in central Stockholm during the year 2017 (Figure 4a). To simulate realistic pedestrian flows over time, these volumes were further refined based on the distribution of pedestrian activity across different days of the week and hours of the day. This approach utilized data from a 2015 Stockholm regional travel behavior survey (Stockholms County, 2016), which includes full-day travel schedules of approximately 11,500 individuals in Stockholm County. Specif-



(a) Average Daily Pedestrian flow of central Stockholm



(b) Distribution of Pedestrian volume across different days of the week and hours of the day in central Stockholm

Figure 4: Sources of pedestrian demand data

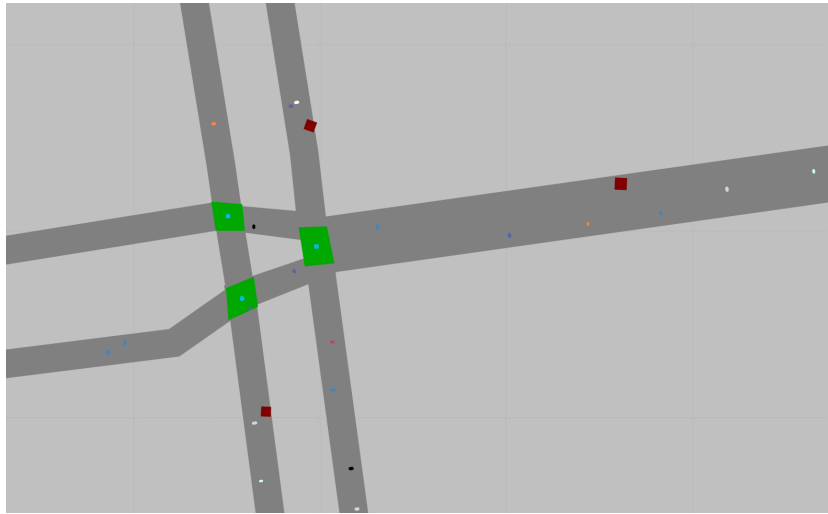


Figure 5: Obstacles (red squares) on the sidewalk network

ically, we focused on trips originating from or directed to the central Stockholm area to derive this distribution (Figure 4b). Based on this distribution, the pedestrian volume for a specific day and time was calculated, and then the corresponding 15-minute flow rates were derived for each segment, enabling the construction of OD matrices for the simulation. The pedestrian population follows the standard composition and features: half are men with speeds uniformly distributed between 3.49–5.83 km/h, and half are women with speeds between 2.56–4.28 km/h.

Obstacles in the simulation play a key role in influencing pedestrian movement patterns. In this study, we model various obstacles to reflect real-world barriers and elements. The obstacle placement is based on the actual street layouts, more specifically the number of sidewalks. Given a percentage, a corresponding share of road segments is selected, and an obstacle of random size is placed at a random location on each. We set up 12 obstacle configurations with the following percentages: 0, 10%, 20%, 30%, 40%, 50% (each repeated twice). The obstacles generated are squares with side lengths randomly varying between 1 and 1.4 meters. Figure 5 illustrates an example of obstacles placed within the sidewalk network.

4.2 Performance analysis

To assess the need of RSP algorithms over conventional shortest path algorithms, we first analyze how optimal paths vary across various simulation scenarios. The conventional shortest paths are computed for 500 OD pairs, ensuring each path includes at least five segments. Results show that only five OD pairs maintain the same path across all scenarios, while 346 have at least 10 different paths, and 33

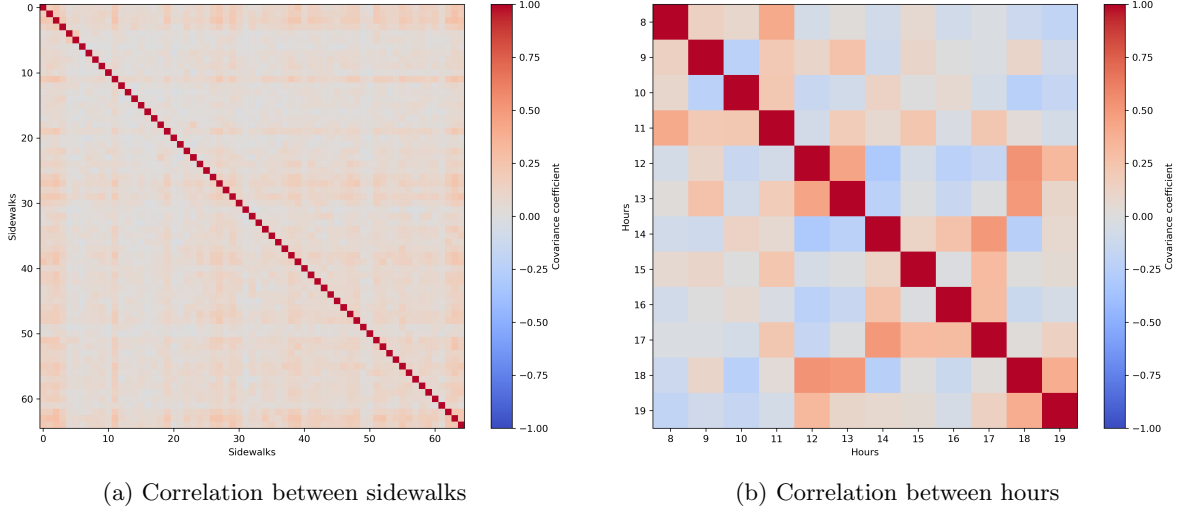


Figure 6: Correlation between segments and between hours

exhibit over 50 different paths. On average, each OD pair has 19.25 unique optimal paths, highlighting the need for robust shortest path approaches.

Before generating uncertainty (or ambiguity) sets, we analyze travel time correlations among segments and across different hours. Figure 6a illustrates the correlation coefficients for each pair of sidewalks. Notably, a weak positive correlation exists among certain pairs of sidewalks. However, the absolute value of the correlation coefficient for 90% of the pairs does not exceed 0.14, and the highest value is only 0.27, indicating a near absence of significant correlation between sidewalks, implying that travel time fluctuations on one sidewalk are relatively independent of those on others. The correlation across various hours is shown in Figure 6b. We aggregate the average travel time over all segments in the network and derive the temporal correlation between different hours. Variations across hours are driven by differences in simulated pedestrian volumes. The results indicate relatively strong temporal correlations, with 10 out of 66 hour pairs exhibiting absolute correlation values above 0.3, and two pairs exceeding 0.5. High correlation during certain hours suggests consistent and predictable travel time patterns, implying reduced temporal uncertainty. While such predictability could benefit the implementation of time-dependent algorithms, we focus here on a time-independent approach for better tractability and transferability.

Based on the low spatial correlation, it is possible to apply the TSC-DS algorithm for SVC, which resolves the over-conservatism caused by high-dimensional data and improves the computational tractability (see Section 3.1.3). The 99 segments are randomly grouped into 49 paired two-dimensional subsets (one subset has three segments), effectively reducing the dimensionality from 99 to 2. While the standard SVC based on 1612 simulated data points would typically yield over 322 SVs, the proposed algorithm reduces such a number to just over 12 SVs. As a result, the average running time for a single origin-destination pair decreases from 11,552 seconds to 13.8 seconds, on a system equipped with an Intel Core i7-1365U processor.

Nevertheless, since sidewalk travel times are not entirely uncorrelated (some segment pairs still exhibit moderate dependencies), we extended the TSC-DS algorithm by incorporating hierarchical clustering to form more meaningful groups. Instead of random grouping, the correlation matrix between segments is used as a distance matrix for hierarchical clustering to produce 49 clusters. Segment pairs are then assigned based on these cluster labels, ensuring that each group contains two segments. This approach accounts for potential inter-segment correlations within each group and is expected to improve the performance of SVC compared to purely random grouping. Other clustering methods, such as K-means with variable group sizes, were tested but performed worse than random pairing and are therefore omitted from further discussion. Both the extended SVC with hierarchical grouping and the original SVC with random grouping are included in the subsequent analysis.

Each method is evaluated across a range of parameter settings, informed by preliminary experiments designed to identify stable and effective configurations. For the MKL-based SVC method, we adopt $M = 16$ basis kernels and set $\mu = 0.2$ based on sensitivity analysis over the range $\mu \in [0.05, 0.5]$,

which showed limited variation in results and justified using a fixed value. The Wasserstein-based DRSP approach involves three parameters: α , ϵ_N , and N . To simplify the comparison and reduce dimensionality, we vary each parameter individually while holding the others constant and identify stable values through preliminary pruning. As a result, we fix $\alpha = 0.3$ and $N = 500$, and vary ϵ_N in the main analysis. The full set of parameter ranges used in the experiments is:

- budgeted uncertainty: $\Gamma \in \{1, 2, \dots, 10\}$;
- ellipsoidal uncertainty: $\lambda \in \{1, 2, \dots, 10\}$;
- SKL-based and MKL-based SVC uncertainty: $v \in \{0.02, 0.04, \dots, 0.2\}$
- Wasserstein-based DRSP: $\epsilon_N \in \{0.01, 0.05, 0.1, 0.2, \dots, 0.8\}$

For the budgeted model, the parameter $\Gamma = 0$ corresponds to free-flow travel times, and the resulting paths correspond to the conventional shortest paths. This case is used as a benchmark for the various approaches.

A five-fold validation is performed to ensure a rigorous performance evaluation of RSP methods. In each fold, 1612 (80%) of the 2016 scenarios are used for training, and 404 (20%) for validation, sampled from the travel time matrix. From the initial 500 OD pairs, the 100 with the highest travel time standard deviation are selected, resulting in 1,656,400 travel cost calculations per fold.

To achieve a comprehensive evaluation of all methods, we adopt three performance criteria as defined by Chassein et al. (2019):

- the average travel time across all OD pairs and scenarios,
- the average worst-case travel time across scenarios for all OD pairs,
- the average of the 5th percentile worst travel times across all scenarios for all OD pairs.

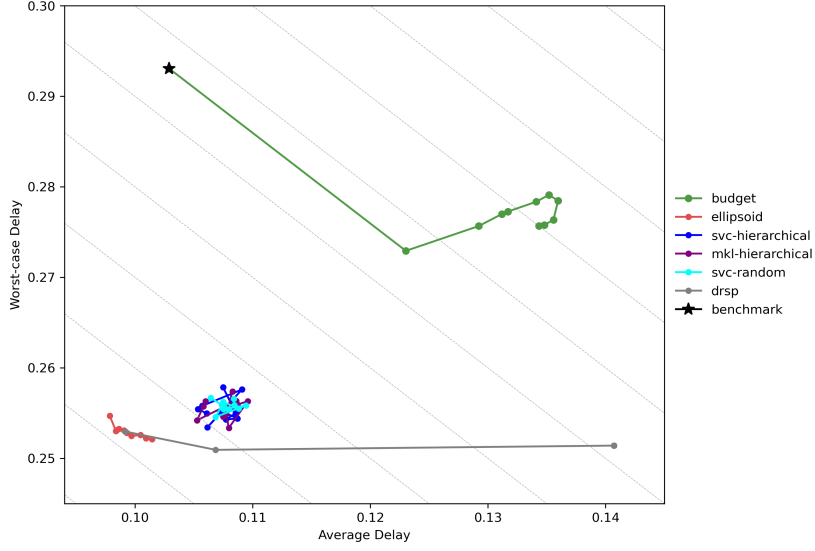
Prior to computing these criteria, the travel time of each OD pair, T_i , is normalized by the free flow travel time of the benchmark path ($\Gamma = 0$), T_{ff} , to minimize the impact of varying distances between different OD pairs. The normalized delay \tilde{D} is then computed as: $\tilde{D} = (T_i - T_{ff})/T_{ff}$. Accordingly, the three performance criteria are referred to as average delay, worst-case delay, and worst 5% delay, respectively.

The performance of various methods under different parameter settings is illustrated in Figure 7. In general, robust paths typically exhibit longer average delay than conventional paths because they are explicitly designed to incorporate uncertainty as worst-case travel times. On the other hand, they significantly reduce travel delay in the most challenging situations. Lower values on both axes indicate better performance; hence, points closer to the lower-left corner represent more desirable trade-offs between efficiency and robustness. To visualize the trade-off between these two KPIs, grid lines with a slope of -1 are included in the figures.

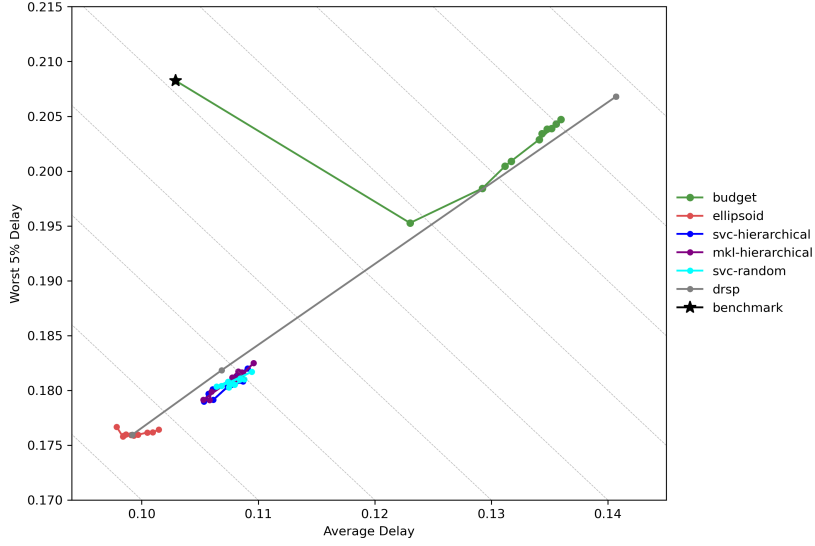
Figure 7a compares average delay and worst-case delay across different methods and parameter settings. All robust methods yield lower worst-case delays than the benchmark, which has an average worst-case delay of 0.293. Under the Budgeted uncertainty set, the best result is achieved with $\Gamma = 1$, reducing the worst-case delay by up to 6.9%. However, increasing Γ leads to overly conservative solutions characterized by poorer performance.

The Ellipsoidal, SKL- and MKL-based SVC, and DRSP perform substantially better. For Ellipsoidal uncertainty, the lowest worst-case delay (14% reduction) is achieved at $\lambda = 10$, but it comes at the cost of the largest average delay. Smaller λ values lead to higher worst-case delays but lower average delays. Notably, the Ellipsoidal method consistently achieves lower average delays across all parameters than the conventional SP, with reductions of up to 4.9%, indicating higher routing efficiency.

The DRSP method achieves the overall lowest worst-case delay (0.251) at $\epsilon_N = 0.1$, but its average delay increases markedly beyond this parameter. For the SVC-based methods, all three variants show comparable overall performance. However, the SKL- and MKL-based extensions, which incorporate hierarchical clustering, outperform the original SVC with random grouping under specific parameter settings ($v = 0.12$ and $v = 0.16$, respectively). They reach maximum reductions in worst-case delay of 13.5% and 13.3% relative to the benchmark.



(a) Average vs. Worst case



(b) Average vs. Worst 5%

Figure 7: Trade-off between three performance criteria

When analyzing performance for the worst 5% travel delays (Figure 7b), the differences between parameter settings are more pronounced. Again, the Ellipsoidal method performs consistently better than the other methods. The DRSP method performs well, but its performance deteriorates sharply as ϵ_N increases, indicating a high sensitivity to parameter selection. Although the SVC-based methods underperform compared to the Ellipsoidal and DRSP approaches, the hierarchical extension shows a more pronounced improvement over the original SVC in reducing the worst 5% of delays.

We integrate the analysis of aggregated results with a more detailed analysis of three performance metrics across individual OD pairs. For a fair comparison, the best-performing parameters for each robust method are selected based on the previous analysis: $\Gamma = 1$ for Budgeted, $\lambda = 3$ for Ellipsoidal, $v = 0.12$ for SKL-based SVC, $v = 0.16$ for MKL-based SVC, $v = 0.16$ for original SVC, and $\epsilon_N = 0.05$ for DRSP. The results illustrated in Figure 8 as box plots, with lower and more compact boxes indicating higher efficiency and robustness.

Figure 8a shows the distribution of average travel delays. All robust methods display greater variability compared to the conventional SP method. Among them, the Ellipsoidal method achieves lower and more concentrated average delays than the other robust approaches. All robust methods outper-

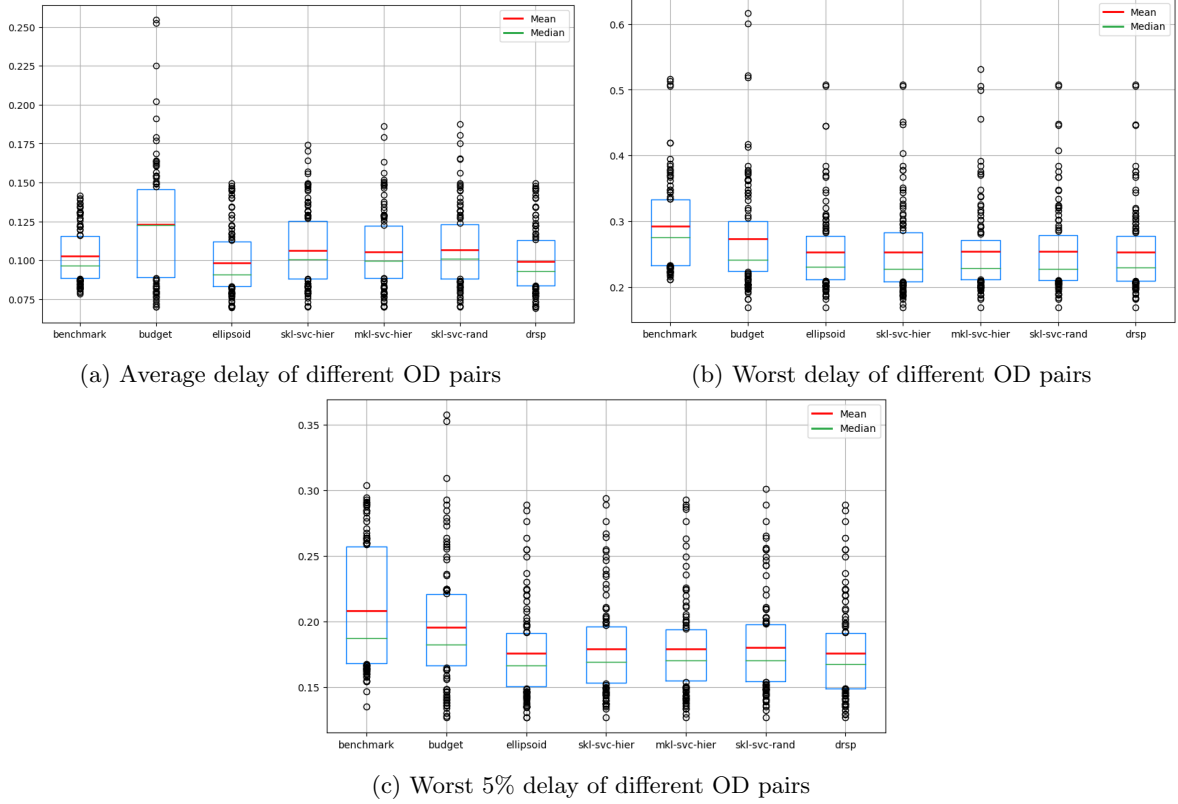


Figure 8: Distribution of three types of uncertainty sets for different OD pairs

form the conventional approach in terms of worst-case delay variability (Figure 8b), with distributions that are both narrower and lower. The Ellipsoidal method stands out with a slightly lower distribution and the lowest average worst-case delay. The advantages of robust methods are even more evident in the worst 5% scenarios, illustrated in Figure 8c. Both the Ellipsoidal and DRSP methods exhibit significantly lower medians and means, along with tighter distributions, indicating strong performance in the most adverse conditions. Although the Budgeted method demonstrates improved robustness over the benchmark for most OD pairs, it performs even worse than the benchmark for certain individual OD pairs, which is not observed with the other robust methods.

These findings indicate that well-tuned robust approaches significantly reduce worst-case delays across OD pairs with high uncertainty, compared to the traditional shortest path method. Among them, the Ellipsoidal and DRSP methods not only outperform other robust methods in terms of worst-case delays, but also achieve lower average delays than the conventional approach. While the Ellipsoidal method performs consistently well across parameters, the DRSP method demonstrates strong performance when properly tuned, highlighting its potential under careful calibration. In addition to strong average performance, their consistent results across individual OD pairs highlight greater stability and practical reliability. The adopted five-fold validation approach guarantees these results can be generalized without overfitting risks.

In contrast with our expectations, the data-driven SVC-based approaches, while outperforming the Budgeted method in terms of robustness, fail to surpass the Ellipsoidal method in either robustness or efficiency. This occurs regardless of the investigated SVC variant (single or multi-kernel). When considering computational cost, this performance gap becomes even more pronounced since the scalability of SVC becomes problematic for large problem sizes. Moreover, the marginal improvement achieved by incorporating hierarchical clustering suggests that addressing weak inter-segment relationships in SVC does not yield substantial gains and is insufficient to outperform the Ellipsoidal or DRSP methods.

One possible explanation lies in the characteristics of the dataset itself. The input data consists of a simulated sidewalk robot travel time matrix which may be relatively "symmetric". Its distribution may be well approximated by an ellipsoid fitted to the observed data, rendering the added complexity of SVC methods unnecessary. Additionally, data-driven methods typically require larger datasets to

effectively learn complex patterns. For applications with more limited data, the Ellipsoid method seems to be more suitable. Further investigation is needed to better understand the impact of dataset size and structure on method performance.

4.3 Sensitivity analysis

In real-world sidewalk robot operations, various design and environmental factors can influence robot performance (respectively discussed in Section 4.3.1 and Section 4.3.2) can affect the comparative advantage of robust methods over the conventional SP approach. To investigate this, a one-way local sensitivity analysis is conducted to evaluate how variations in robot design features and environmental factors impact the performance of robust methods.

Each factor is varied independently across three configurations, which include a “normal” case aligned with the main experiments in Section 4.2, except for obstacle placement, which is adjusted to the sidewalk edges to avoid unrealistic blockages and slightly reduce travel time variability.

Each case is simulated under 2016 scenarios as before (see Section 4.1). The resulting travel time matrices are fed into the same performance evaluation framework described in Section 4.2, consisting of the following KPIs: average delays, worst-case delays, and worst 5% delays. To clearly illustrate the improvement of robust methods over the SP approach, we report the difference in each performance criterion between the SP and robust methods, where higher values indicate greater delay reduction and, thus, better performance.

Since our previous analyses identified the Ellipsoidal and DRSP methods as the most promising robust approaches, we limit the sensitivity analysis to these two. We re-evaluate them using the same parameter tuning ranges as in the main experiments:

- Ellipsoidal uncertainty: $\lambda \in \{1, 2, \dots, 10\}$;
- DRSP: $\epsilon_N \in \{0.01, 0.05, 0.1, 0.2, \dots, 0.8\}$, with fixed $\alpha = 0.3$ and $N = 500$.

4.3.1 Impacts of robot design features

Key robot design features, including desired speed, width, and navigation behavior, can affect the relative performance of robust methods compared to the SP approach. The trade-offs between average travel delays and worst travel delays improvements across various robot design configurations.

Three distinct levels of robot desired speed are considered in Figure 9a: 5 km/h (normal), 7.5 km/h, and 10 km/h, representing a range from slower to relatively faster-moving robots. As the desired speed increases, the benefits of robust methods diminish. Specifically, the maximum improvement in worst-case delay drops from 4.5% at 5 km/h to just 0.3% at 10 km/h, while the gain in average delay decreases from 0.5% to only 0.1% over the same range. This suggests that faster-moving robots experience lower variability in travel time, reducing the relative advantage of incorporating robustness.

In Figure 9b, we evaluate robot widths of 50 cm (normal), 75 cm, and 100 cm, covering the range from narrow to wide designs. The results show a clear performance increase, with worst-case delay improvements increasing from 4.5% (50 cm) to 6.0% (100 cm). Average delay reductions also improve slightly. Although wider robots may face greater difficulty navigating narrow or obstructed sidewalks, robust models demonstrate a stronger ability to manage this added uncertainty than the SP method.

Robot navigation behavior is categorized into three profiles: conservative, normal, and aggressive, each modeled using the SFM with distinct parameter settings listed in Table 1. Figure 9c shows that conservative robots gain the most from robust planning. The maximum improvement in worst-case delay reaches 7.4% under conservative behavior, compared to just 0.6% for aggressive behavior. Similarly, the maximum improvement in average delay is 1.8% for conservative behavior, while only 0.06% for aggressive behavior. This result suggests that robust methods are especially beneficial when robot behavior leads to increased interaction with pedestrians or greater routing variability.

Overall, the robust approaches show higher reliability and efficiency than the SP model for most robot design settings investigated. These advantages are more pronounced for slower, wider, and more conservative robots.

Across all the robot design configurations, the Ellipsoidal method generally performs better than the DRSP method, with only occasional overlaps. Moreover, its lower performance variation suggests that ellipsoidal uncertainty set-based RSP may have a greater stability and easier parameter tuning.

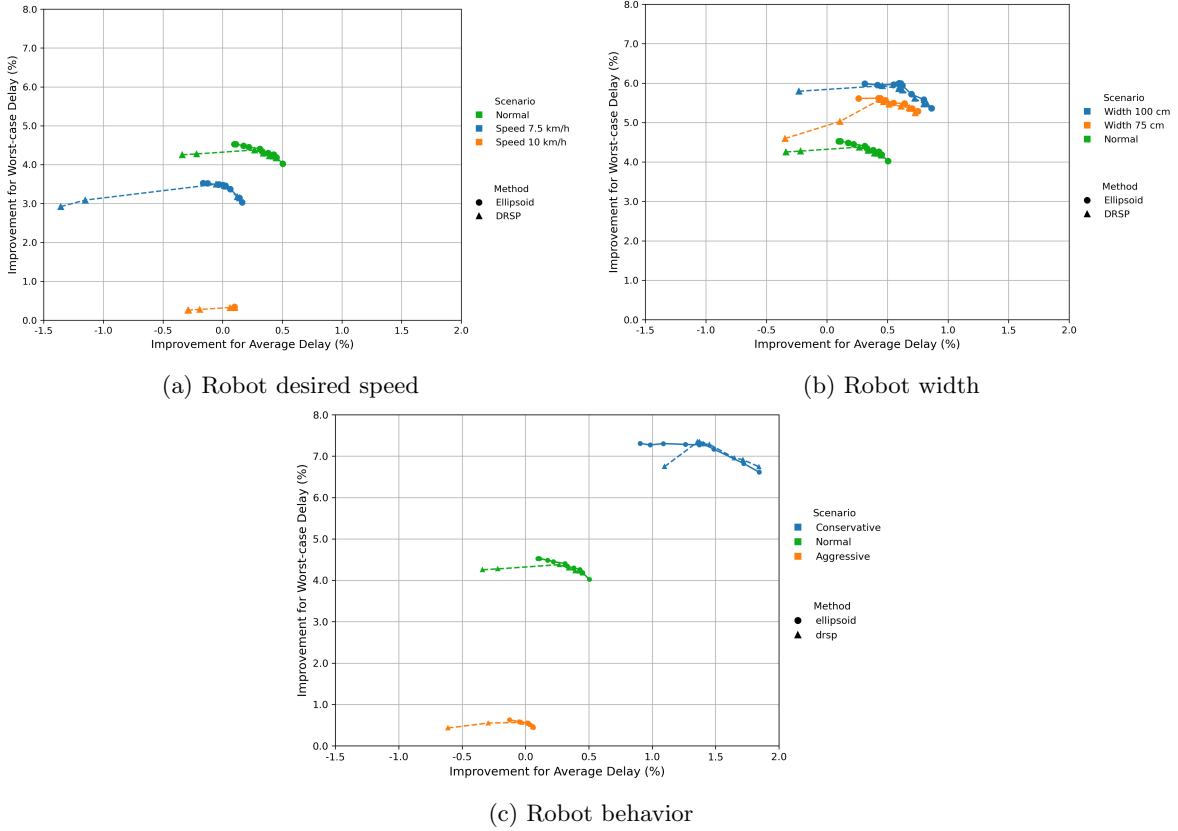


Figure 9: Performance improvement of selected robust methods under various robot design conditions

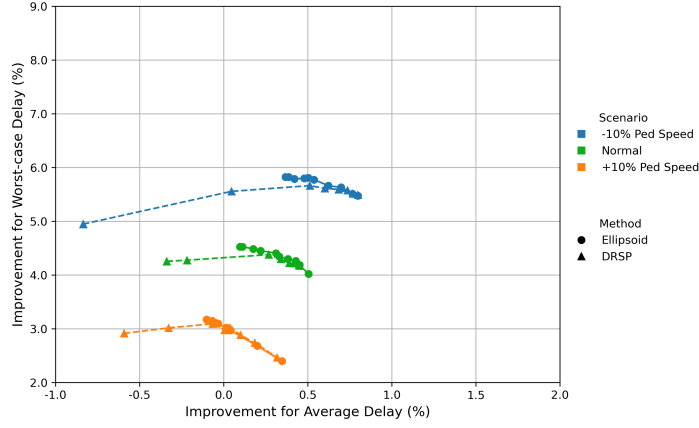
4.3.2 Impacts of environmental factors

Environmental conditions such as weather and pedestrian density can significantly affect sidewalk robot navigation. Weather conditions significantly influence pedestrian speed on sidewalks (Giannoulaki and Christoforou, 2024) due to reduced visibility, balance challenges, and surface conditions. For example, rain, wind, or snow typically slow movement, while light rain or extreme heat may incentivize pedestrians to walk faster to minimize exposure. To simulate these irregular weather conditions, pedestrian speed is adjusted by $\pm 10\%$, based on empirical evidence from Fossum and Ryeng (2021); Liang et al. (2020). While VISWALK does not allow direct simulation of weather, its effects can be indirectly represented by adjusting relevant parameters. In addition, while the original set of experiments realistically accounts for hourly and daily pedestrian volume variations, extraordinary circumstances such as special events, holidays, and tourist peaks can cause occasional surges in foot traffic. These conditions are simulated by uniformly increasing the pedestrian volumes across the network by 50% and 100%. Using the same methodology applied to the robot design features, the improvements for average travel delays and worst travel delays achieved by robust methods over the SP method are derived and presented in Figure 10.

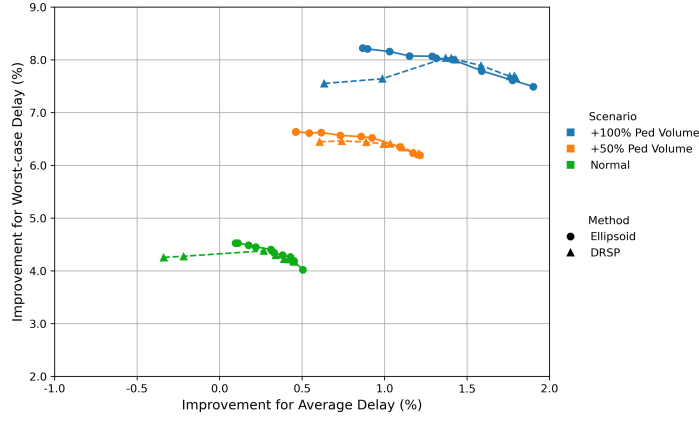
The relative benefits of robust routing diminish with increased average pedestrian speed. Specifically, the maximum improvement in worst-case delay declines from 5.8% under a 10% reduction in pedestrian speed and to 3.2% under a 10% increase. Similarly, the improvement in average delay drops from 0.8% to 0.35% across the same range. In contrast, increased pedestrian volumes lead to greater gains from robust methods. When pedestrian volume is doubled, the maximum improvement in worst-case delay rises from 4.5% in the normal case to 8.2%, while the gain in average delay rises from 0.5% to 1.9%.

These results highlight the robustness and reliability of the selected models, whose performance over the SP approach, increases significantly even under moderate surges in pedestrian volumes and adverse weather conditions which reduce the average pedestrian speed.

The two robust methods exhibit similar trends to those observed in Section 4.3.1. The Ellipsoidal



(a) Pedestrian speed



(b) Pedestrian volume

Figure 10: Performance improvement of selected robust methods under various environmental factors

method consistently outperforms the DRSP method, indicating that when reliability is prioritized over efficiency, the Ellipsoidal method offers superior performance across all scenarios. When the average delay is the primary focus, the two robust methods show comparable performance.

4.4 Operational Insights

The analyses presented in this study provide several actionable insights for logistics operators deploying sidewalk delivery robots in urban settings. Robust routing approaches (particularly the Ellipsoidal and DRSP methods) will bring significant benefits in complex environments characterized by pedestrian congestion and variability. These gains can be amplified during weather events that reduce pedestrian speed. For operators managing time-sensitive services like on-demand food delivery and grocery delivery, robust routing approaches can help improve service reliability and customer satisfaction. These considerations easily apply to many scenarios sharing similar characteristics with Stockholm city center, such as compact urban form, high pedestrian volumes, and variable weather conditions.

The sensitivity analyses also suggest that certain robot designs inherently benefit more from robust routing. While several designs are currently being tested by manufacturers, it is unlikely that the maximum allowed speeds will be higher than pedestrian speeds (around 5 km/h) for safety reasons. It is also probable that manufacturers, at least in the early stages, will adopt more conservative navigation behavior. These characteristics increase travel time variability, reinforcing the operational value of robust routing approaches in real-world deployments.

From an efficiency standpoint, operators may consider hybrid strategies where robust route planning is activated only during periods characterized by higher uncertainty (e.g., peak hours, poor weather). This targeted deployment can reduce computational requirements while securing reliability when it

matters most. Finally, data needs and tuning complexity should not be neglected in the specific method selection.

5 Conclusion

Sidewalk delivery robots represent a promising opportunity for enhancing last-mile distribution in urban settings. However, their efficiency in environments characterized by high pedestrian volumes and unforeseen obstacles is relatively unknown. This study addresses this gap by investigating route planning for sidewalk robots by explicitly formulating the problem as a robust route planning task and integrating it with the simulation of sidewalk pedestrian flows.

Four robust approaches are analyzed: two "traditional" formulations (Budgeted and Ellipsoidal uncertainty), and two data-driven methods (the SVC-based method and DRSP approach). The application of SVC in robust optimization is particularly noteworthy, as it merges machine learning and optimization techniques to model uncertainty in high-dimensional, complex data settings. To address computational issues, we implement the TSC-DS algorithm and propose an extension using hierarchical clustering to generate more meaningful feature groupings. Pedestrian simulation is adopted to realistically account for travel time variability due to different uncertainties, including environmental and operational ones.

A comparative analysis with the conventional SP approach shows that robust approaches consistently lead to more reliable and efficient routing decisions for the sidewalk. The majority of the analyzed 500 OD pairs exhibit significant variability, highlighting the importance of robust methods for the sidewalk delivery route planning. Of all the methods tested, the Ellipsoidal and well-tuned DRSP methods achieve the best overall performance. Although the SVC-based method offers high flexibility by avoiding prior assumptions on the uncertainty structure, it does not perform better than Ellipsoidal or DRSP methods likely due to limited complexity and size of the problem studied.

Finally, we perform a systematic sensitivity analysis to assess the benefits of the two most efficient robust models (Ellipsoidal and DRSP) under various robot design and environmental conditions. The results further confirm the advantages of robust approaches, particularly for delivery robots with larger width, lower design speeds, and more conservative navigation behaviors. Moreover, these advantages are even greater in dense pedestrian settings and when average walking speeds decrease, underscoring the value of robust methods under challenging real-world conditions.

The analyses of this study shed light on different questions, while leaving others for future research. The simulated travel time matrix may exhibit regularities, making the distribution of travel times, and ultimately favoring standard methods like the ellipsoidal. The performance of the data-driven methods, including both SVC and DRSP, could improve with access to larger and more diverse training datasets. The assumption of full travel time observability in the simulation-based approach is also ideal since in real-world applications, trip data from sidewalk delivery robots is likely to be sparser and incomplete. Future work should focus on methods capable of handling partial observability. Scalability challenges of robust routing methods arising with larger networks are another promising direction of research. Finally, the robust routing problem should be investigated in other case studies involving multiple modes, such as shared spaces and multi-modal networks, to support broader development.

Acknowledgments

The study was partly funded by Digital Futures under the ISMIR project, *Investigating Sidewalks' Mobility and Improving it with Robots*.

A Derivation of RSP model based on SVC

This appendix provides the detailed derivation of the RSP model based on SVC, which is presented in Section 3.1. The SKL-based SVC with the WGIK was proposed by Shang et al. (2017). It utilizes SVs to define boundaries in feature space, grouping data points into clusters by finding the smallest sphere that encloses them. This approach not only manages correlated uncertainties, resulting in asymmetric uncertainty sets, but it also features adaptive complexity, embodying a nonparametric approach. The convex polyhedral uncertainty set generated can ensure the robust counterpart problem of the same type as the deterministic problem.

The SKL-based SVC model uses a nonlinear mapping $\phi(u)$ to project observations into high-dimensional feature space, and then finds the smallest hyperplane that encloses all data. The mapping function $\phi(u)$ is complicated but it can be calculated indirectly by evaluating kernel function $K(\mathbf{u}^i, \mathbf{u}^j) = \phi(\mathbf{u}^i)^T \phi(\mathbf{u}^j)$. The dual formulation of SVC model is given below:

$$\begin{aligned} \min_{\alpha} \quad & \sum_{i=1}^N \sum_{j=1}^N \alpha_i \alpha_j K(\mathbf{u}^i, \mathbf{u}^j) - \sum_{i=1}^N \alpha_i K(\mathbf{u}^i, \mathbf{u}^i) \\ \text{s.t.} \quad & 0 \leq \alpha_i \leq 1/Nv, i = 1, \dots, N \\ & \sum_{i=1}^N \alpha_i = 1 \end{aligned} \quad (25)$$

A regularization parameter $v \in (0, 1]$ is introduced to control the conservatism degree of the uncertainty set. It is an upper bound on the fraction of outliers and a lower bound on the fraction of support vectors (Shang et al., 2017). The kernel function WGIK is calculated in Eq. (26):

$$K(\mathbf{u}, \mathbf{v}) = \sum_{k=1}^n l_k - \|\mathbf{Q}(\mathbf{u} - \mathbf{v})\|_1 \quad (26)$$

where \mathbf{Q} is a weighting matrix generated from covariance matrix $\mathbf{\Sigma} = \mathbf{\Sigma}^{-\frac{1}{2}}$. The unbiased estimation of the covariance matrix $\mathbf{\Sigma}$ can be obtained in Eq.(27)

$$\mathbf{\Sigma} = \frac{1}{N-1} \left[\sum_{k=1}^n \mathbf{u}^i (\mathbf{u}^i)^T - \left(\sum_{k=1}^n \mathbf{u}^i \right) \left(\sum_{k=1}^n \mathbf{u}^i \right)^T \right] \quad (27)$$

The kernel parameters l_k should satisfy Eq.(28), then the kernel matrix \mathbf{K} can be positive definite. Note that if Eq.(28) is satisfied, no matter what the value of l_k is, it will not affect the induced SVC model.

$$l_k > \max_{1 \leq i \leq N} \mathbf{q}_k^T \mathbf{u}^i - \min_{1 \leq i \leq N} \mathbf{q}_k^T \mathbf{u}^i \quad (28)$$

After solving the model (25) with kernel function WGIK, the index sets of all support vectors and boundary support vectors can be defined according to the following Eqs. (29)(30)

$$SV = \{i | \alpha_i > 0, \forall i\} \quad (29)$$

$$BSV = \{i | 0 < \alpha_i < 1/Nv, \forall i\} \quad (30)$$

Besides, an explicit expression of the data-driven uncertainty set can be derived as a set of linear inequalities:

$$U^{SVC} = \left\{ \mathbf{u} \left| \begin{array}{l} \exists \mathbf{v}_i, i \in SV \text{ s.t.} \\ \sum_{i \in SV} \alpha_i \cdot \mathbf{1}^T \mathbf{v}_i \leq \theta \\ -\mathbf{v}_i \leq \mathbf{Q}(\mathbf{u} - \mathbf{u}^i) \leq \mathbf{v}_i, \forall i \in SV \end{array} \right. \right\} \quad (31)$$

where $\theta = \sum_{i \in SV} \alpha_i \|\mathbf{Q}(\mathbf{u}^{i'} - \mathbf{u}^i)\|_1$, i' can be any index in BSV , and \mathbf{v}_i are auxiliary variables introduced.

In order to apply the above SVC-based uncertainty set into robust shortest path problem, Eq.(2) can be simplified by moving the inner objective function into a constraint

$$\begin{aligned} \min_{\mathbf{x} \in X, b} \quad & b \\ \text{s.t.} \quad & \max_{\mathbf{u} \in U} \mathbf{u}^T \mathbf{x} \leq b \end{aligned} \quad (32)$$

The left hand side (LHS) of constraint in Eq. (32) can be reformulated into the linear programming model Eq.(33) by replacing the uncertainty set as linear inequalities constraints in Eq.(31).

$$\begin{aligned} \max_{\mathbf{u}, \mathbf{v}_i} \quad & \mathbf{u}^T \mathbf{x} \\ \text{s.t.} \quad & \sum_{i \in SV} \alpha_i \cdot \mathbf{1}^T \mathbf{v}_i \leq \theta \\ & -\mathbf{v}_i \leq \mathbf{Q}(\mathbf{u} - \mathbf{u}^i) \leq \mathbf{v}_i, \forall i \in SV \end{aligned} \quad (33)$$

By introducing Lagrange multipliers λ_i , μ_i , η and β , the model (33) can be translated into its dual form:

$$\begin{aligned} \min_{\lambda_i, \mu_i, \eta} \quad & \sum_{i \in SV} (\mu_i - \lambda_i)^T \mathbf{Q} \mathbf{u}^i + \eta \theta \\ \text{s.t.} \quad & \sum_{i \in SV} \mathbf{Q}(\lambda_i - \mu_i) + \mathbf{x} = \mathbf{0} \\ & \lambda_i + \mu_i = \eta \cdot \alpha_i \cdot \mathbf{1}, \lambda_i, \mu_i \in \mathbb{R}_+^n, \forall i \in SV \\ & \eta \geq 0 \end{aligned} \quad (34)$$

We know that, for any feasible λ_i , μ_i , η , and optimal solution \mathbf{u} , \mathbf{v}_i to the primal problem (33), there always exists $\sum_{i \in SV} (\mu_i - \lambda_i)^T \mathbf{Q} \mathbf{u}^i + \eta \theta \geq \mathbf{u}^T \mathbf{x}$. Moreover, according to Shang et al. (2017), the objective values of the primal and dual coincide due to strong duality of LP. Thus, the Eq.(32) can be written as Eq.(35):

$$\begin{aligned} \min_{\mathbf{x}, \lambda_i, \mu_i, \eta} \quad & b \\ \text{s.t.} \quad & \sum_{i \in SV} (\mu_i - \lambda_i)^T \mathbf{Q} \mathbf{u}^i + \eta \theta \leq b \\ & \sum_{i \in SV} \mathbf{Q}(\lambda_i - \mu_i) + \mathbf{x} = \mathbf{0} \\ & \lambda_i + \mu_i = \eta \cdot \alpha_i \cdot \mathbf{1}, \lambda_i, \mu_i \in \mathbb{R}_+^n, \forall i \in SV \\ & \eta \geq 0 \\ & \mathbf{x} \in X \end{aligned} \quad (35)$$

Substituting X with constraints for shortest path problem, the final model for robust shortest path problem with WGIK-SVC-based uncertainty set can be defined as follows:

$$\begin{aligned} \min_{x_{pq}, \lambda_i, \mu_i, \eta} \quad & b \\ \text{s.t.} \quad & \sum_{i \in SV} (\mu_i - \lambda_i)^T \mathbf{Q} \mathbf{u}^i + \eta \theta \leq b \\ & \sum_{i \in SV} \mathbf{Q}(\lambda_i - \mu_i) + \mathbf{x} = \mathbf{0} \\ & \lambda_i + \mu_i = \eta \cdot \alpha_i \cdot \mathbf{1}, \forall i \in SV \\ & \sum_{\{q: (p,q) \in A\}} x_{pq} - \sum_{\{q: (q,p) \in A\}} x_{qp} = \begin{cases} 1 & \text{if } p = s \\ -1 & \text{if } q = t \\ 0 & \text{otherwise} \end{cases} \\ & \lambda_i, \mu_i \in \mathbb{R}_+^n, \eta \geq 0, x_{pq} \in \{0, 1\} \end{aligned} \quad (36)$$

References

- Alves Pessoa, A., Di Puglia Pugliese, L., Guerriero, F., and Poss, M. (2015). Robust constrained shortest path problems under budgeted uncertainty. *Networks*, 66(2):98–111.
- Anvari, B. and Wurdemann, H. A. (2020). Modelling social interaction between humans and service robots in large public spaces. In *2020 IEEE/RSJ International Conference on Intelligent Robots and Systems (IROS)*, pages 11189–11196.
- Ben-Tal, A. and Nemirovski, A. (1998). Robust convex optimization. *Mathematics of Operations Research*, 23(4):769–805.
- Ben-Tal, A. and Nemirovski, A. (1999). Robust solutions of uncertain linear programs. *Operations Research Letters*, 25(1):1–13.
- Bertsimas, D. and Brown, D. (2009). Constructing uncertainty sets for robust linear optimization. *Operations Research*, 57:1483–1495.
- Bertsimas, D. and Sim, M. (2003). Robust discrete optimization and network flows. *Mathematical Programming*, 98:49–71.
- Bishop, C. (2016). Swiss post trials robot parcel deliveries in bern. <https://www.thelocal.ch/20160823/swiss-post-trials-robot-parcel-deliveries-in-bern>.
- Bliss, J. (2023). On airport delivery & investor revenue demands. <https://www.ottomate.news/p/on-airport-delivery-and-investor>.
- Boysen, N., Fedtke, S., and Schwerdfeger, S. (2021). Last-mile delivery concepts: a survey from an operational research perspective. *Or Spectrum*, 43(1):1–58.
- Boysen, N., Schwerdfeger, S., and Weidinger, F. (2018). Scheduling last-mile deliveries with truck-based autonomous robots. *European Journal of Operational Research*, 271(3):1085–1099.
- Burns, J. (2016). Domino’s pizza robot making deliveries in australia. <https://www.forbes.com/sites/janetwburns/2016/03/18/dominos-pizza-robot-is-making-deliveries-in-australia/>.
- Chassein, A., Dokka, T., and Goerigk, M. (2019). Algorithms and uncertainty sets for data-driven robust shortest path problems. *European Journal of Operational Research*, 274(2):671–686.
- Chassein, A. B. and Goerigk, M. (2015). A new bound for the midpoint solution in minmax regret optimization with an application to the robust shortest path problem. *European Journal of Operational Research*, 244(3):739–747.
- Chen, C., Demir, E., Huang, Y., and Qiu, R. (2021). The adoption of self-driving delivery robots in last mile logistics. *Transportation Research Part E: Logistics and Transportation Review*, 146:102214.
- Cheng, J., Lisser, A., and Letournel, M. (2013). Distributionally robust stochastic shortest path problem. *Electronic Notes in Discrete Mathematics*, 41:511–518.
- Coldewey, D. (2019). Kiwi’s food delivery bots are rolling out to 12 more colleges. <https://techcrunch.com/2019/04/25/kiwis-food-delivery-bots-are-rolling-out-to-12-new-colleges/>.
- De Maio, A., Ghiani, G., Laganà, D., and Manni, E. (2024). Sustainable last-mile distribution with autonomous delivery robots and public transportation. *Transportation Research Part C: Emerging Technologies*, 163:104615.
- Dokka, T. and Goerigk, M. (2017). An experimental comparison of uncertainty sets for robust shortest path problems. *arXiv preprint arXiv:1704.08470*.
- Du, Y., Hetherington, N. J., Oon, C. L., Chan, W. P., Quintero, C. P., Croft, E., and Machiel Van der Loos, H. (2019). Group surfing: A pedestrian-based approach to sidewalk robot navigation. In *2019 International Conference on Robotics and Automation (ICRA)*, pages 6518–6524.

- Ensafian, H., Zare Andaryan, A., Bell, M. G., Glenn Geers, D., Kilby, P., and Li, J. (2023). Cost-optimal deployment of autonomous mobile lockers co-operating with couriers for simultaneous pickup and delivery operations. *Transportation Research Part C: Emerging Technologies*, 146:103958.
- Ferrer, G., Garrell, A., and Sanfeliu, A. (2013a). Robot companion: A social-force based approach with human awareness-navigation in crowded environments. In *2013 IEEE/RSJ International Conference on Intelligent Robots and Systems*, pages 1688–1694.
- Ferrer, G., Garrell, A., and Sanfeliu, A. (2013b). Social-aware robot navigation in urban environments. In *2013 European Conference on Mobile Robots*, pages 331–336.
- Fossum, M. and Ryeng, E. O. (2021). The walking speed of pedestrians on various pavement surface conditions during winter. *Transportation Research Part D: Transport and Environment*, 97:102934.
- Gehrke, S. R., Phair, C. D., Russo, B. J., and Smaglik, E. J. (2023). Observed sidewalk autonomous delivery robot interactions with pedestrians and bicyclists. *Transportation Research Interdisciplinary Perspectives*, 18:100789.
- Ghiasvand, M. R. and Rahmani, D. (2023). A novel weighted data-driven robust optimization approach for creating adjustable uncertainty sets. *Computers & Chemical Engineering*, 178:108390.
- Giannoulaki, M. and Christoforou, Z. (2024). Pedestrian walking speed analysis: A systematic review. *Sustainability*, 16(11).
- Goerigk, M. and Kurtz, J. (2023). Data-driven robust optimization using deep neural networks. *Computers & Operations Research*, 151:106087.
- Goerigk, M. and Schöbel, A. (2015). Algorithm engineering in robust optimization. *arXiv preprint arXiv:1505.04901*.
- Gruden, C., Ištoka Otković, I., Šraml, M., et al. (2022). Three-step performance assessment of a pedestrian crossing time prediction model. *Transactions on transport sciences*, 12(3):13–21.
- Han, B., Shang, C., and Huang, D. (2021). Multiple kernel learning-aided robust optimization: Learning algorithm, computational tractability, and usage in multi-stage decision-making. *European Journal of Operational Research*, 292(3):1004–1018.
- Heimfarth, A., Ostermeier, M., and Hübner, A. (2022). A mixed truck and robot delivery approach for the daily supply of customers. *European Journal of Operational Research*, 303(1):401–421.
- Helbing, D. and Molnar, P. (1995). Social force model for pedestrian dynamics. *Physical review E*, 51(5):4282.
- Hossain, M. (2022). Self-driving robots: A revolution in the local delivery. https://cmr.berkeley.edu/2022/04/self-driving-robots-a-revolution-in-the-local-delivery/?utm_source=chatgpt.com.
- Jennings, D. and Figliozzi, M. (2019). Study of sidewalk autonomous delivery robots and their potential impacts on freight efficiency and travel. *Transportation Research Record*, 2673(6):317–326.
- Johansson, A., Helbing, D., and Shukla, P. (2008). Specification of a microscopic pedestrian model by evolutionary adjustment to video tracking data. *arXiv preprint arXiv:0810.4587*.
- Kasperski, A. and Zielinski, P. (2016). *Robust Discrete Optimization Under Discrete and Interval Uncertainty: A Survey*, volume 241, pages 113–143. Springer International Publishing.
- Ketkov, S. S., Prokopyev, O. A., and Burashnikov, E. P. (2021). An approach to the distributionally robust shortest path problem. *Computers & Operations Research*, 130:105212.
- Kumawat, S., Dudeja, C., and Kumar, P. (2021). An extensive review of shortest path problem solving algorithms. In *2021 5th International Conference on Intelligent Computing and Control Systems (ICICCS)*, pages 176–184.

- Kwon, C., Lee, T., and Berglund, P. G. (2013). Robust shortest path problems with two uncertain multiplicative cost coefficients. *Naval Research Logistics (NRL)*, 60.
- Lemardel , C., Estrada, M., Pag s, L., and Bachofner, M. (2021). Potentialities of drones and ground autonomous delivery devices for last-mile logistics. *Transportation Research Part E: Logistics and Transportation Review*, 149:102325.
- Li, J., Ensafian, H., Bell, M. G., and Geers, D. G. (2021). Deploying autonomous mobile lockers in a two-echelon parcel operation. *Transportation Research Part C: Emerging Technologies*, 128:103155.
- Liang, S., Leng, H., Yuan, Q., Wang, B., and Yuan, C. (2020). How does weather and climate affect pedestrian walking speed during cool and cold seasons in severely cold areas? *Building and Environment*, 175:106811.
- Liu, D., Yan, P., Pu, Z., Wang, Y., and Kaisar, E. I. (2021). Hybrid artificial immune algorithm for optimizing a van-robot e-grocery delivery system. *Transportation Research Part E: Logistics and Transportation Review*, 154:102466.
- Marks, M. (2019). Robots in space: Sharing the sidewalk with autonomous delivery vehicles. *Available at SSRN 3347466*.
- Murray, C. C. and Chu, A. G. (2015). The flying sidekick traveling salesman problem: Optimization of drone-assisted parcel delivery. *Transportation Research Part C: Emerging Technologies*, 54:86–109.
- Ning, C. and You, F. (2018). Data-driven decision making under uncertainty integrating robust optimization with principal component analysis and kernel smoothing methods. *Computers & Chemical Engineering*, 112:190–210.
- PTV (2023). *PTV VISSIM 2023 User Manual*. PTV group.
- Roytvand Ghiasvand, M., Rahmani, D., and Moshref-Javadi, M. (2024). Data-driven robust optimization for a multi-trip truck-drone routing problem. *Expert Systems with Applications*, 241:122485.
- Shang, C., Huang, X., and You, F. (2017). Data-driven robust optimization based on kernel learning. *Computers & Chemical Engineering*, 106:464–479. ESCAPE-26.
- Shang, C. and You, F. (2018). Robust optimization in high-dimensional data space with support vector clustering. *IFAC-PapersOnLine*, 51(18):19–24. 10th IFAC Symposium on Advanced Control of Chemical Processes ADCHEM 2018.
- Sharan, S., Surya, R., and Suchithra, R. (2022). Autonomous robot-driven deliveries: A review of recent developments and future directions. *Transportation research part E: logistics and transportation review*, 165:102834.
- Shi, X., Xue, S., Feliciani, C., Shiwakoti, N., Lin, J., Li, D., and Ye, Z. (2021). Verifying the applicability of a pedestrian simulation model to reproduce the effect of exit design on egress flow under normal and emergency conditions. *Physica A: statistical mechanics and its applications*, 562:125347.
- Simoni, M. D., Kutanoglu, E., and Claudel, C. G. (2020). Optimization and analysis of a robot-assisted last mile delivery system. *Transportation Research Part E: Logistics and Transportation Review*, 142:102049.
- Stockholm County (2016). Resvanor i stockholms l n 2015. ‘Travel habits in Stockholm County’; in Swedish. <https://miljobarometern.stockholm.se/content/docs/tema/trafik/resvanor/RVU-stockholms-lan-2015.pdf>.
- Stockholm County (2025). Clean air zone class 3. <https://trafik.stockholm/en/traffic-safety-and-rules/clean-air-zones/clean-air-zone-class-3/>.
- Stockholms County (2017). Fl deskarta f r g ngtrafik. ‘G ngfl deskarta  ver city’; in Swedish. <https://miljobarometern.stockholm.se/content/Trafikrelaterat/G%C3%A5ngfl%C3%B6deskarta%20City%202017.pdf>.

- Truong, X.-T. and Ngo, T. D. (2017). Toward socially aware robot navigation in dynamic and crowded environments: A proactive social motion model. *IEEE Transactions on Automation Science and Engineering*, 14(4):1743–1760.
- Ulmer, M. W. and Streng, S. (2019). Same-day delivery with pickup stations and autonomous vehicles. *Computers & Operations Research*, 108:1–19.
- Wahlberg, A. (2024). Uber and avride are bringing delivery robots and autonomous vehicles to city streets. <https://foodondemand.com/10082024/uber-and-avride-announce-delivery-robot-and-autonomous-vehicle-partnership/>.
- Wang, Z., You, K., Song, S., and Shang, C. (2019). Data-driven distributionally robust shortest path problem using the wasserstein ambiguity set. In *2019 IEEE 15th International Conference on Control and Automation (ICCA)*, pages 1391–1396.
- Wang, Z., You, K., Song, S., and Zhang, Y. (2020). Wasserstein distributionally robust shortest path problem. *European Journal of Operational Research*, 284(1):31–43.
- Yang, Y., Quan, X., and Sun, Y. (2023). Enhanced social force model for service robots in various environments: Calibration and simulation. In *2023 IEEE 13th International Conference on CYBER Technology in Automation, Control, and Intelligent Systems (CYBER)*, pages 89–94.